View metadata, citation and similar papers at core.ac.uk
brought to you by CORE
provided by NASA Technical Reports Server

A Global Ozone Climatology from Ozone Soundings via Trajectory Mapping: A Stratospheric Perspective

J. J. Liu[1,2,3], D. W. Tarasick[1], V. E. Fioletov[1], C. McLinden[1], T. Zhao[4], S. Gong[1], C. Sioris[1], J. J. Jin[5], G. Liu[6], and O. Moeini[7]

[1]Science and Technology Branch, Environment Canada, 4905 Dufferin Street, Downsview, Ontario, Canada M3H 5T3

[2]Department of Geography and Planning, University of Toronto, 100 St. George Street, Toronto, Ontario, Canada M5S 3G3

[3]Nanjing University, Nanjing, Jiangsu, China, 210093

[4]Nanjing University of Information Science & Technology, Nanjing, Jiangsu, China, 210044

[5]Universities Space Research Association, and Global Modeling and Assimilation Office, Goddard Space Flight Center, NASA, Greenbelt, MD, USA

[6]Space Sciences Laboratory, University of California, Berkeley, California, USA, 94720

[7]Department of Earth and Space Science & Engineering, York University, 4700 Keele Street, Toronto, Ontario, M3T 1P3

Submitted to *Atmospheric Chemistry and Physics*

12 June 2013

[1]Corresponding author:

Department of Geography and Planning, University of Toronto,

100 St. George Street, Room 5047, Toronto, Ontario, Canada M5S 3G3

E-mail:janejj.liu@utoronto.ca, Tel: (416) 946-8257, FAX: (416) 946-3886

Abstract

This study explores a domain-filling trajectory approach to generate a global ozone climatology from relatively sparse ozonesonde data. Global ozone soundings comprising 51,898 profiles at 116 stations over 44 years (1965-2008) are used, from which forward and backward trajectories are calculated from meteorological reanalysis data, to map ozone measurements to other locations and so fill in the spatial domain. The resulting global ozone climatology is archived monthly for five decades from the 1960s to the 2000s on a grid of 5°×5°×1 km (latitude, longitude, and altitude), from the surface to 26 km altitude. It is also archived yearly from 1965 to 2008. The climatology is validated at 20 selected ozonesonde stations by comparing the actual ozone sounding profile with that derived through trajectory mapping of ozone sounding data from all stations except the one being compared. The two sets of profiles are in good agreement, both individually with correlation coefficients (r) between 0.975 and 0.998 and root mean square (RMS) differences of 87 to 482 ppbv, and overall with $r = 0.991$ and an RMS of 224 ppbv. The ozone climatology is also compared with two sets of satellite data, from the Satellite Aerosol and Gas Experiment (SAGE) and the Optical Spectrography and InfraRed Imager System (OSIRIS). The ozone climatology compares well with SAGE and OSIRIS data in both seasonal and zonal means. The mean differences are generally quite small, with maximum differences of 20% above 15 km. The agreement is better in the northern hemisphere, where there are more ozonesonde stations, than in the southern hemisphere; it is also better in the middle and high latitudes than in the tropics where reanalysis winds are less accurate. This ozone climatology captures known features in the stratosphere, as well as seasonal and decadal variations of these features. Compared to current satellite data, it offers more complete high latitude coverage as well as a much longer record. The climatology shows clearly the depletion of ozone from the 1970s to the

45 mid 1990s and ozone recovery in the lower stratosphere in the 2000s. When this climatology is
46 used as the upper boundary condition in an Environment Canada operational chemical forecast
47 model, the forecast is improved in the vicinity of the upper troposphere–lower stratosphere
48 (UTLS) region. As this ozone climatology is neither dependent on *a priori data* nor
49 photochemical modeling, it provides independent information and insight that can supplement
50 satellite data and model simulations of stratospheric ozone.

1 Introduction

Ozone is an important trace gas in the atmosphere, playing a significant role in atmospheric chemical, dynamical, and radiative processes. In the stratosphere, emissions of human-produced ozone depleting substances led to a substantial ozone decline that has been reversed by the implementation of the Montreal Protocol in 1987 and its subsequent amendments (WMO, 2003, 2007). Identifying stratospheric ozone recovery and assessing the impact of ozone changes on climate are important issues that have attracted considerable attention (e.g., Randel and Wu, 1999; Weatherhead and Andersen, 2006; Waugh et al., 2009; Eyring et al., 2010; Ziemke and Chandra, 2012). Stratospheric ozone can also impact chemistry and dynamics in the troposphere, both via direct exchange and the Brewer-Dobson circulation (e.g., Holton et al., 1995; Stohl et al., 2003) and via effects on planetary wave propagation and global climate (Baldwin and Dunkerton, 2001; Gillett and Thompson, 2003).

An understanding of the distribution of stratospheric ozone and its long-term changes is a critical step to assessing the interactions between ozone variability and climate change. Satellite observations have advantages of consistent quality and global coverage, but suffer from biases between different, or successive instruments and limited vertical or horizontal resolution depending on the measurement approach. Considerable effort has been made previously to develop ozone climatologies, typically combining satellite measurements from one or more instruments with other data sources, often ozonesondes. These datasets are either meridionally and vertically resolved (two dimensions in latitude and altitude, e. g., Fortuin and Kelder, 1998; Lamsal et al., 2004; McPeters et al., 2007; Randel and Wu, 2007; Hassler et al., 2008; Jones et al., 2009; McLinden et al., 2009; McPeters and Labow, 2012) or of ozone column that is horizontally resolved (two dimensions in latitude and longitude, e. g., Ziemke et al., 2005, 2011).

Stratospheric ozone climatologies in two or three dimensions have also been developed from chemistry-climate model simulations (e.g., Eyring et al., 2010; SPARC CCMVal, 2010). Although considerable advances have been made in the past decade to improve model representations of ozone transport and chemistry, uncertainties remain with regard to parameterizations, radiation transport schemes, and simulation of the Brewer-Dobson circulation, as well as prediction of the late-spring breakup of the Antarctic vortex and of the Antarctic ozone hole (e. g., SPARC CCMVal, 2010; Forster et al. 2011; Wang and Waugh, 2012).

In this study, we explore a different approach to develop a long-term ozone climatology from global ozonesonde data for satellite and model *a priori*, satellite and climate model data validation, troposphere-stratosphere exchange, and atmospheric climate-chemistry interaction research. Ozone soundings have the advantages of long-term and quasi-global coverage, high accuracy, and high vertical resolution but are sparse in space and time. Given ozone's long lifetime of weeks to months in the lower stratosphere (e.g., Jacob, 1999; Liu and Ridley, 1999), a measurement of ozone mixing ratio at one place and time generally provides a good estimate of ozone mixing ratio in that same air parcel several days before or after. It is therefore possible to extend sparse ozonesonde measurements and to fill the gaps in the spatial domain by trajectory calculations, assuming the ozone mixing ratio along each trajectory path is constant. This is a technique that has been used successfully with other stratospheric data (Sutton et al., 1994; Newman and Schoeberl, 1995; Morris et al., 2000), and with ozone data in both the stratosphere and troposphere. Stohl et al. (2001) used trajectory statistics to extend one year of MOZAIC (Measurement of Ozone and Water Vapour by Airbus In-service Aircraft) ozone measurements into a 4-season ozone climatology at 10° longitude by 6° latitude and three vertical heights. Trajectory mapping has also been used to fill gaps in satellite MLS (Microwave Limb Sounder)

ozone data in the stratosphere in order to calculate the tropospheric residual ozone column (Schoeberl et al., 2007). Tarasick et al. (2010) developed high resolution (1°×1°×1 km in latitude, longitude, and altitude) tropospheric ozone fields for North America from ozonesonde data from the INTEX (Intercontinental Transport Experiment) and ARCTAS (Arctic Research of the Composition of the Troposphere from Aircraft and Satellites) campaigns. This has been recently extended to global tropospheric ozonesonde data by Liu et al. (2013).

Our study is aimed at (1) developing a global long-term ozone climatology from ozonesondes in 3 dimensions (latitude, longitude, and altitude), (2) validating this dataset against independent ozonesondes and satellite observations, (3) characterizing the stratospheric ozone distribution and its decadal and seasonal variabilities, and (4) illustrating applications of this dataset in providing evidence of ozone recovery and in improving simulations of tropospheric ozone.

In the following, Section 2 describes the methodology of trajectory mapping and the input ozonesonde data. Section 3 describes the validation of the trajectory-mapped dataset with ozonesonde data and the comparison between this dataset and satellite datasets from SAGE (the Satellite Aerosol and Gas Experiment) and OSIRIS (the Optical Spectrography and InfraRed Imager System). In Section 4, the variation of stratospheric ozone at different time scales is characterized. Section 5 discusses the timing of stratospheric ozone recovery, based on this ozone climatology, and shows the improvement in the simulation of tropospheric ozone in an air quality forecast model when this climatology is used as the upper boundary condition. Conclusions are provided in Section 6.

2 Methods

2.1 Global Ozonesonde Data

The global ozonesonde data used herein were acquired from the World Ozone and Ultraviolet Radiation Data Centre (WOUDC), which is one of five World Data Centres of the Global Atmosphere Watch programme of the World Meteorological Organization. The WOUDC operates a scientific archive, providing ozone data to the international scientific community (Wardle et al., 1998; Hare et al. 2007). Table 1 describes these stations, including their geolocations (latitude, longitude, and elevation), operation periods, and the total number of profiles used in this study. The stations' geolocations are illustrated in Figure 1a, showing their non-uniform distribution around the globe. There are more stations in the northern hemisphere (NH) than in the southern hemisphere (SH), and more stations over Europe and North America than over Asia. Large gaps appear over China and eastern Russia. The total number of available stations is 47 in the 1970s (Figure 1b). This number gradually increases with time. In the 2000s, there are 57 stations (Figure 1c) with more coverage in the tropics, South Asia, East Asia, the Arctic, and the Antarctic. Overall, we employ 51,898 ozone soundings globally at 111 stations, in different periods (Table 1) over 44 years from 1965 to 2008.

Most of the profiles are from the electrochemical concentration cell (ECC)-type ozonesonde, which was introduced in the early 1970s and adopted by a majority of stations in the global network by the early 1980s. Virtually all the data in the most recent decade are from ECC sondes. The remainder are from Brewer-Mast (BM) sondes (currently still in use at one site), the Japanese KC96 sonde, and the Indian sonde. Prior to the early 1990s, three stations in Europe (Praha, Lindenberg and Legionowo) flew the GDR sonde. A majority of the data before 1980 is from BM sondes or similar (both the GDR and Indian sondes are similar in design to the BM sonde). A small amount of data is available in the early 1960s from carbon-iodine sondes

143 (similar to the KC sondes) and from Regener sondes (which operated by the chemiluminescent
144 reaction of ozone with luminol).

145 When properly prepared and handled, ECC ozonesondes have a precision of 3-5% (1-σ)
146 and an absolute accuracy of about 5% in the stratosphere (Kerr et al., 1994; Smit et al., 2007;
147 Deshler et al., 2008; Liu et al., 2009). The ozone sensor response time (e^{-1}) of about 25 seconds
148 gives the sonde a vertical resolution of about 100 metres for a typical balloon ascent rate of 4
149 m/s. Two types of ECC ozonesondes are in current use, the 2Z model manufactured by EnSci
150 Corp. and the 6A model manufactured by Science Pump, with minor differences in construction
151 and some variation in recommended concentrations of the potassium iodide sensing solution and
152 of its phosphate buffer. The maximum variation in stratospheric response resulting from these
153 differences is likely of the order of 2-3% (Smit et al., 2007).

154 The precision of other sonde types is somewhat poorer, at about 5-10% (Kerr et al., 1994;
155 Smit et al., 1996). In early intercomparisons (Attmannspacher and Dütsch, 1970, 1981) the
156 Indian and the GDR sonde showed significantly poorer precision than other sonde types.

157 The largest systematic differences between sondes are in the lower stratosphere, where
158 the BM and GDR sondes gave readings about 5-10% lower than the ECC and KC sondes in early
159 intercomparisons (Attmannspacher and Dütsch, 1970; 1981). In later intercomparisons (Kerr et
160 al., 1994; Smit et al., 1996; Deshler et al., 2008) the KC sondes have shown a low bias of about
161 5% in the lower stratosphere, and the BM has generally shown a low bias as well. The Indian
162 sonde has generally shown little bias in the lower stratosphere, but somewhat lower precision
163 than the other non-ECC sondes. Regener sondes were used regularly for only a brief period in
164 the 1960s, as they showed somewhat erratic response (Hering and Dütsch, 1965).

In the middle and upper stratosphere below 26 km differences in sonde response are small. Overall, between the tropopause and 26 km the precision of the various sonde types in recent decades is generally within ±5%, and any systematic biases between them or compared to other ozone sensing techniques are smaller than ±5% (World Climate Research Programme, 1998).

2.2 Trajectory Calculation and Global Ozone Mapping

To prepare for trajectory modelling, the ozone mixing ratio profile for each sounding was integrated into 26 vertical levels at 1-kilometre resolution from sea level. Ozone measurements above 26 km were excluded because of their higher uncertainties (e.g., Fioletov et al., 2006). Trajectories for all 26 levels were calculated using the Hybrid Single-Particle Lagrangian Integrated Trajectory (HYSPLIT) model (version 4.9) (Draxler and Hess, 1998, Draxler et al., 2012), available from the Air Resources Laboratory, National Oceanic and Atmospheric Administration (NOAA) (http://www.arl.noaa.gov /HYSPLIT_info.php). HYSPLIT is driven by the reanalysis meteorological data from the National Centers for Environmental Prediction/National Center for Atmospheric Research (NCEP/NCAR) (Kalnay et al., 1996). These data are available from 1965 to the present. Both forward and backward trajectories for 4 days (96 hours) were calculated for 51,898 ozone soundings and the trajectory positions were stored.

Ozone mixing ratios in the 26 levels from each sounding were assigned to the corresponding trajectory positions along the forward and backward paths every 6 hours for 4 days (32 positions for each level). Then, the trajectory-mapped data were binned at intervals of 5º latitude and 5º longitude, at each 1-km altitude, and averaged. This bin size is less than the

typical ozone correlation length in the stratosphere of about 1000-1500 km (Liu et al., 2009). Two different altitude coordinates were employed for this binning, and so two sets of maps were produced, one whose vertical coordinate is altitude above sea level, and the other altitude above ground level. A global ozone climatology of monthly means for each altitude was generated for each decade from the 1960s to the 2000s. The climatology is also archived yearly from 1965 to 2008 at the same horizontal and vertical resolutions. Figure 1 illustrates the improved spatial coverage if trajectory mapping is used. The trajectory mapping greatly spreads out the ozone information along the trajectory paths, increasing the spatial domain to include most of the globe.

Most atmospheric models using assimilated meteorological data produce tropopause heights that are more accurate than climatology. Using an ozone climatology that includes a climatological tropopause with such models can produce, in effect, spurious stratospheric intrusions as air in the upper troposphere (when the actual tropopause is high) is assigned stratospheric values of ozone (e.g., Makar et al., 2010). The opposite effect can occur when the actual tropopause is low. For this reason, we generated three ozone climatology datasets. The first dataset is a conventional climatology that uses ozonesonde data in both troposphere and stratosphere, while in the second and third dataset, the stratospheric ozone climatology and tropospheric ozone climatology are generated separately with trajectories originating exclusively from the stratosphere and the troposphere, respectively. The explicitly separated troposphere and stratosphere, which overlap in the upper troposphere-lower stratosphere (UTLS) region, are intended to be used for model *a priori* where an atmospheric model determines the tropopause location itself. This paper focuses on characterization and validation of the first and second datasets, while the tropospheric climatology is discussed in a separate paper (Liu et al., 2013).

3. Validation and Comparison with Independent Ozone Observations

3.1 Comparison with Ozonesonde Profiles

To test the trajectory methodology, the actual ozone profile at selected stations was compared with that produced by the trajectory mapping using the ozone soundings at all stations except the one being compared. Figure 2 shows examples of such comparison in the NH winter and summer months (January and July) in 1990s at four stations: Boulder (40.1° N, 105.3° W, 1689 m), Hohenpeissenberg (47.8° N, 11.0° E, 975 m), Uccle (50.8° N, 4.0° E, 100 m), and Eureka (80.0° N, 86.2° W, 310 m). The paired profiles shown are in reasonable agreement. Seasonal variation is well captured in the trajectory-derived ozone profiles. The correlation coefficient (r) between the two datasets is between 0.950 and 0.999. Biases are between -170 and +80 ppbv, while RMS differences range from 60 to 340 ppbv.

Globally, twenty stations were selected (Table 2, Figure 1a), with a range of latitude from 71° S (Neumayer) to 80° N (Eureka), and longitude from 171° W (Samoa) to 178° E (Fuji), and in altitude from near sea level (Tahiti) to 1745 m (Nairobi). There are 10 stations each in the northern and southern hemispheres, while the number of stations is 9 and 11, respectively, in the eastern and western hemisphere.

In Figure 3, the decadal monthly mean ozone abundance from ozonesonde data at selected stations is compared with that from trajectory mapping without input from the station being tested, for all the 20 stations in the 1990s and 2000s. Overall, the correlation coefficient between the two datasets is 0.99. The overall bias is negligible, at 1.2 ppbv, while the RMS difference is 224 ppbv. For individual stations, the correlation coefficient ranges between 0.975 and 0.999 and the RMS differences between 87 and 482 ppbv.

3.2 Comparison with SAGE Ozone Data

The satellite instrument SAGE (McCormick et al., 1989) was designed to measure ozone in the stratosphere where most ozone resides. The SAGE mission expanded over 20 years starting from SAGE I onboard AEM2 (Application Explorer Mission) in 1979. SAGE I was in operation until 1981. SAGE II, on board ERBS (Earth Radiation Budget Satellite), was in operation from 1984-2005. SAGE uses the highly accurate solar occultation technique and has a vertical resolution of less than 1 km. Ozone is derived from measurements in the spectral range of 0.385-1.020 μm (Cunnold et al., 1989). In the absence of clouds, SAGE can detect some layers in the middle and upper troposphere after a significant improvement in the algorithms (Kent et al., 1993). Wang et al. (2002) compared SAGE II with ozonesonde data and found that SAGE tends to slightly overestimate ozone (less than 5%) between 15 and 20 km altitude and to systematically underestimate ozone in the troposphere by approximately 30% between 2 and 8 km altitude. This is consistent with the comparisons we make with the trajectory-mapped data in Figure 4 below.

This study uses SAGE I version 7.0 and SAGE II version 6.2 (Wang et al., 2006). Vertical profiles are reported in number density at 1-km resolution from 0.5 km to 60.5 km. Each profile is matched with temperature and pressure from NMC/NCEP (National Meteorological Centre/National Centre for Environment Protection) to derive ozone mixing ratio from the surface to 26 km (McLinden et al., 2009). The comparison with SAGE data is conducted here in two ways.

Firstly, profiles from the ozone climatology were compared with SAGE and ozonesonde data vertically. About 1400 SAGE profiles that coincide with ozonesonde profiles, from 1979 to 2005, were extracted. Each pair of SAGE and ozonesonde profiles was matched with the profile from the ozone climatology in the corresponding month, decade, and 5°×5° latitude-longitude

bin. That is, the comparisons between ozonesonde and SAGE profiles were made at the same location and time, while ozonesonde profiles were compared with those from the ozone climatology at the same location, month, and decade. Figure 4 shows the vertical distribution of the mean relative differences in the 1990s in NH summer (JJA) and winter (DJF) by four latitudinal zones. Above 15 km, mean differences from the ozone climatology are mostly <10%, as are SAGE-sonde differences. Below 15 km, the ozone climatology is closer to ozonesondes than SAGE. The distribution of the bias for vertical profiles of SAGE is consistent with previous studies (e.g., Wang et al., 2002; Fioletov et al., 2006). The comparison between the climatology and ozonesondes is better in the summer than in the winter, and better at higher latitudes (45-90° N, 45-90° S) than at lower latitudes (0-45° N, 0-45° S). This appears to be largely the case for SAGE as well. To some extent, the difference profiles of the climatology from sondes in Figure 4 are similar to the corresponding SAGE-sonde difference profiles, which may indicate that they are largely due to sampling issues with the sondes.

Secondly, decadal monthly mean from SAGE were gridded at the same 3-dimensional resolution as the ozone climatology (5° × 5°×1 km in latitude, longitude, and altitude). The two datasets, for the same time period, are compared by grid cell, along with ozonesonde data. Figure 5 compares the three datasets by season, taking data at grid cells where all the data are available in the 1990s and the 2000s.

In general, the trajectory-derived ozone climatology agrees well with ozonesondes (left panels) and the degree of scatter shows little variation with season. The scatter is due to imperfections in the wind fields, as well as measurement error in the original sonde data. The SAGE-ozonesonde correlation appears reasonably good for the four seasons (middle panels), although the degree of scatter is larger than that for the ozone climatology. The ozone

climatology correlates well with SAGE data in all seasons (right panels) with RMS errors that are about the same as the SAGE-sonde comparison (middle panels). Most notable is that the leftmost panels show much less scatter (smaller RMS errors and higher *r*) in all seasons than the two comparisons involving SAGE data.

The same data points are divided into six 30º latitude zones (Figure 6). The climatology is closely correlated with independent ozonesondes, with $r > 0.98$ in all cases. The SAGE-ozonesonde correlations (Figure 6, right panels) show more scatter than the ozone climatology-ozonesonde correlations in all six latitude zones. As in Figure 5, the ozone climatology-SAGE correlations (not shown) are similar to the SAGE-sonde correlations. Table 3 lists statistics for the ozone climatology and SAGE data in NH winter and summer seasons and 3 altitudes in the 1990s and the 2000s. Both datasets capture the altitude-dependent seasonal variations. The ozone climatology and SAGE data are well-correlated at 14.5 km with $r \sim 0.9$. The correlation becomes smaller at higher altitudes. At 19.5 km, the correlation coefficient is ~0.8 for both winter and summer in the 1990s and the 2000s. At 24.5 km the correlation is poorer, reflecting the fact that the RMS/Mean is lower. The mean ozone mixing ratio from the climatology dataset is higher than SAGE at 14.5 km (similar to the SAGE-sonde bias in Figure 4) but shows little bias at higher altitudes. The RMS difference between the two datasets decreases with altitude from about 30% at 14.5 km to about 15-20% at 24.5 km.

Figure 7 shows the relative difference ($=[O_{3(Clim)} - O_{3(SAGE)}]/\text{mean}[O_{3(Clim)},O_{3(SAGE)}]$, in %) in NH winter and summer in the 1990s at 19.5 km and 24.5 km. The comparison covers parts of the globe where both datasets are available. At 19.5 km, the ozone climatology shows significant positive bias relative to SAGE data in several regions, including the region downwind of the east coast of the United States and over the Atlantic ocean in the southern hemisphere and the

Antarctic. There are also evident negative biases over mountains in North and South America, Greenland and the Tibetan region. The magnitude of differences is large at 19.5 km (ranging from -100% to 100%), in part perhaps because the ozone gradient with altitude is largest here (Figure 2). At 24.5 km, differences are smaller, ranging from -40% to 40%. Differences are smaller in summer than in winter (Table 3). While the negative biases over mountains may be due to error in the vertical motion fields of the trajectory model, the positive biases noted do not appear to be related to topography. A comparison of individual sonde stations to SAGE (not shown) suggests that they may be due to individual station biases, promulgated by the trajectory mapping.

3.3 Comparison with OSIRIS Ozone Data

OSIRIS is onboard the Swedish/Canadian/French/Finnish Odin satellite, which was launched into a polar, sun-synchronous orbit at 600 km in February 2001 (Murtagh et al., 2002; Llewellyn et al., 2004). OSIRIS can scan the Earth's limb at tangent heights from 10 to 70 km, covering 82.2° S to 82.2°N. The spectrograph measures scattered sunlight from 280–800 nm, with ~1 nm spectral resolution. The field of view is about 1.288 arc min in the vertical direction, equivalent to ~1 km height at the tangent point. The overall accuracy is within 10% between 15 to 35 km altitudes (von Savigny et al., 2003). The mean bias of OSIRIS from coincident SAGE measurements is less than 2% between 18 km to 53 km (Degenstein et al., 2009).

From 2002 to 2010, 5,900,889 data points from OSIRIS were matched with ozone values from this ozone climatology, each pair being in the same month in the 2000s at the same location within the range of a grid (5° ×5° ×1 km in latitude, longitude, and altitude). The 5,900,889 pairs of data were compared by season (Figure 8) and by latitudinal zone (Figure 9). Overall, the two

datasets agree reasonably well (Figures 8a, 9a and 9b). By season, the two datasets agree better above 20 km (relative difference < 10%) than lower altitudes (Figure 8a). The agreement is best in NH summer and fall (maximum relative difference < 5%) and poorest in winter (maximum relative difference < 20%) (Figure 8a). Both datasets can generally capture profile variation with season in both magnitude and profile shape (Figures 8b and 8c). The largest relative difference (≈20%) appears in winter over the UTLS region where ozone values from OSIRIS are smaller than those from this ozone climatology (Figures 8a-8c). However, it should be noted that the very strong gradients of ozone concentration with height in this region imply that an altitude bias of as little as 100 m (which could be introduced by the response time of the ascending ozonesonde) could account for this difference. Examined by latitude zone (Figures 9a and 9b), the largest relative differences (again, ~20%) are found below 20 km, in the 0-45° latitude range in both hemispheres. The climatology is closer to OSIRIS from 45° to 90°N, where there is greater density of sonde data, with a relative difference less than 7%. Global mean profiles for different latitudinal zones are very similar to each other in the two datasets, with higher ozone in higher northern and southern latitudes at the same altitude (Figures 9c and 9d).

4 Global Ozone Distribution

4.1 Long-term Climatology

Figure 10 shows the latitude-altitude distribution of the ozone climatology averaged from the 1970s to the 2000s. The trajectory mapped ozone climatology can generally capture the steep ozone changes (<100 to >500 ppbv) in the vicinity of the tropopause over all latitudes. Near 25 km, the ozone climatology is lower at the poles than at lower latitudes. This distribution is similar to that from SAGE data (e.g., Fioletov, 2008).

350 The mean ozone distribution from the 1970s to the 2000s at 19.5 km is shown in Figure
351 11a. In order to fill the remaining gaps (~ 1%) and to reduce small-scale "noise", the
352 climatological average values obtained from the mapping are fitted to a linear combination of
353 spherical functions (Figure 11b). Ozone concentration increases with latitude from ~500 ppbv in
354 the tropics to ~4000 ppbv at the poles, reflecting the influence of the Brewer-Dobson circulation.
355 Moreover, the ozone climatology shows significant longitudinal variation. In the northern
356 hemisphere, Figure 11 shows a wave-like pattern with high ozone over the northernmost parts of
357 North America and eastern Asia, as also found by Stohl et al. (2001), who attributed this feature
358 to the quasi-permanent troughs over the continents (e.g., Fleagel and Businger, 1980). In the
359 southern hemisphere, ozone appears higher over the Antarctic continent.
360
361 **4.2 Decadal Variability**
362 The distribution of ozone at 19.5 km is shown by decade from the 1970s to the 2000s in Figure
363 12. The large gaps in the tropics and in the middle latitudes of the southern hemisphere in the
364 1970s are largely filled in by the SHADOZ program (Southern Hemisphere ADditional
365 OZonesondes, Thompson et al., 2003a, 2003b, 2007) starting from the 1990s (Figures 1b and
366 1c). The global ozone distribution shows some consistent features in the four decades, as
367 described in section 4.1 for the long-term mean. The decadal variability is striking in both
368 hemispheres. Table 4 shows the decadal ozone variation in January and July for the globe, the
369 Arctic (60-90° N), and the Antarctic (60-90° S), averaged by only taking values from the grid
370 cells where ozone data are available in all the four decades. All regions show ozone depletion
371 from the 1970s to the 1990s and ozone recovery in the 2000s. The decadal variation is larger in
372 the winter season than in the summer season in both hemispheres, presumably because chlorine
373 is activated in polar winter. At the 25 km level, the variation is even larger (not shown).

374

375 **4.3 Seasonal Variability**

376 Figure 13 shows the seasonal variability of ozone in the 1990s at 19.5 km, demonstrating that
377 there are sufficient data to separate the seasonal variability. The seasonal variation at this level
378 resembles the variation in total ozone (e.g., Fioletov, 2008). The latitudinal gradient (lower
379 ozone in the equator and higher ozone in the middle and high latitudes) is well captured with a
380 maximum in spring and a minimum in fall. In the northern hemisphere, the spring ozone
381 maximum over the Canadian Arctic is evident. Another high ozone region in the winter and
382 spring is located over northernmost eastern Asia. This is more obvious in the 2000s (not shown),
383 because of ozone recovery in the stratosphere. Both maxima can be also partly seen in the SAGE
384 data up to 60° N (not shown). In the southern hemisphere, ozone starts to accumulate over the
385 South Pole in the SH summer (DJF), gradually increases in abundance and area in SH fall
386 (MAM) and reaches a maximum in the SH winter (JJA). In the SH spring (SON), with
387 heterogeneous destruction of ozone, ozone over the South Pole reaches a minimum, leaving a
388 band of high ozone between 30° and 60° S. This feature is reflected in the dip in the ozone
389 contours at 30°-55° S in Figure 10 above 20 km. It should be regarded with caution, however, as
390 there are relatively few ozone sounding stations in this latitude range (Figure 1), and so most of
391 the information comes via relatively long trajectories, with correspondingly larger uncertainties
392 (see also Figure 14). In addition, the lack of radiosounding stations in this region must also
393 increase the relative uncertainty in the winds in the NCEP database that are used to calculate
394 trajectories. Nevertheless, we note that a similar dip in the ozone contours is seen at 40°-60° N,
395 where ozonesonde data are most abundant. The smoothed ozone fields shown in the right panels
396 of Figure 13 are gap-filled and have reduced small-scale variation and reduced extrema. Seasonal
397 variability in the 2000s (not shown) is similar to that in the 1990s.

398

399 **4.4 Data Coverage and Standard Errors**

400 As shown in Figure 12, the trajectory-mapped coverage is improved after the 1980s. The
401 coverage at 19.5 km averaged over 12 months is 34% in the 1970s, increasing to 52% in the
402 1980s and to ~70% in the 1990s and the 2000s (Table 5). The coverage at higher or lower
403 altitudes is about the same as at this altitude. The average number of samples is around 20-25 per
404 grid cell and there are no large differences in this number between decades or among layers. The
405 averaged standard error is about 6-7% of the mean at 19.5 km and about 4-5% of the mean at
406 24.5 km (Note that standard error is calculated simply from all data points in a grid cell.
407 Depending on the wind speed, some cells may contain more than one value from an individual
408 trajectory, and so the standard error calculation will be biased low). Seasonally, most missing
409 data are in low latitudes (Figure 14). In the NH summer, data are also missing over northeast
410 Asia. In the SH summer (DJF), there are large gaps over South America and the Atlantic Ocean
411 and some regions in the eastern Pacific Ocean. As there are more stations in North America and
412 Europe (Figure 1), the number of samples per cell is the largest over these regions. In the NH
413 winter, there is a band at mid-latitudes (40-70° N) with a large number of samples.
414 Consequently, the standard error of the mean is low in the region. In the southern hemisphere
415 between 40-70° S, with fewer stations, the standard errors are higher, due to the smaller number
416 of samples. This ozone climatology was generated with 4-day forward and backward trajectories.
417 We also explored 6-day trajectories and found a general increase in data coverage and a decrease
418 in the standard error with the 6-day runs. For example, at 19.5 km in January, the coverage
419 increases from 68% to 80% and the mean standard error decreases from 4.8% to 4.7%. Future
420 studies may use additional data sources (e.g., SAGE and OSIRIS data) and improved trajectory

methods (e.g., using a variable time step in the stratosphere and troposphere) to eliminate data gaps and enhance accuracy.

5 Applications

In the following we present two examples of applications of the ozone climatology.

5.1 Stratospheric Ozone Recovery

Following the implementation of the Montreal Protocol and its amendments, there has been considerable interest in tracking the expected recovery of stratospheric ozone, including the dates when ozone may return to its 1960 and 1980 levels and to full ozone recovery, i.e., no longer influenced by human-produced ozone depleting substances (ODSs) (e.g., Weatherhead and Andersen, 2006; Shepherd and Jonsson, 2008; Waugh et al., 2009; Eyring et al., 2010; Ziemke and Chandra, 2012). Ozone recovery remains a challenging issue because of the complexity of the natural variability of ozone, as well as the complex impact of greenhouse-gas induced climate change and the removal of atmospheric ODSs owing to the Montreal Protocol. Eyring et al. (2010) analyzed results from 17 chemistry-climate models and predicted that global stratospheric ozone will return to its 1980 and 1960 levels by ~2025 and ~2040 respectively. Ziemke and Chandra (2012) suggested an earlier recovery of stratospheric ozone on the basis of their analysis of OMI (Ozone Monitoring Instrument) satellite data. Some studies have suggested that ozone recovery would be larger at higher latitudes than lower latitudes (Weatherhead and Andersen, 2006; Ziemke and Chandra, 2012).

Here we analyze ozone time series in the stratosphere using the yearly averaged ozone climatology. Only data from grid points where ozone values are available in all years from 1970 to 2007 are employed to avoid biases due to data sampling. Using this criterion, the northern hemisphere from 30° N to 90° N is a region with data coverage exceeding 70%. Data coverage in

445 other regions is somewhat lower. Figure 15 shows the annual area-weighted mean ozone
446 between 30° N and 90° N at 21.5 km (~50 hPa) and 24.5 km (~40 hPa), along with
447 corresponding 3-year running means. Ozone depletion before the mid-1990s is evident at both
448 levels (as well as in between, not shown). Turnaround at both levels is in 1996. By 2005, ozone
449 was about half-way to returning to its pre-1980 value at both altitudes. This figure is quite
450 similar to Figure 16a of Ziemke and Chandra (2012) which also shows ozone recovery starting
451 from the mid-1990s. The shape of the ozone variation in Figure 15a is also similar to that in
452 Waugh et al. (2009, in their Figure 2c) in a simulation. Weatherhead and Andersen (2006)
453 merged total column ozone data from TOMS (the Total Ozone Mapping Spectrometer) and
454 SBUV/2 (the Solar Backscattered Ultraviolet) satellite instruments and found the lowest ozone
455 values during 1993-1997 over 30° N to 80° N, which also is similar to our results. Their results
456 imply faster recovery in the northern part of the northern hemisphere than is indicated by some
457 atmospheric models (Weatherhead and Andersen, 2006). Figure 15 supports this conclusion,
458 from an independent ozone data source.
459
460 **5.2 Upper Boundary Conditions for Tropospheric Ozone Simulations in Chemistry Models**
461 Previous studies have demonstrated the importance of upper boundary conditions to accurate
462 modeling of tropospheric ozone in regional chemical forecast models (Tarasick et al., 2007;
463 Makar et al., 2010, and references therein). The Canadian Global Environmental Multiscale
464 meteorology model (GEM) has been coupled with the Modelling Air quality and CHemistry
465 (MACH) system (Talbot et al., 2009) to operationally predict tropospheric ozone in a global
466 uniform 1°×1° horizontal resolution. The GEM-MACH global model was used for the CalNex
467 (California Research at the Nexus of Air Quality and Climate Change) field campaign in 2010.
468 The forecasted ozone fields during the campaign from May 10 to June 20, 2010 were evaluated

by applying upper boundary conditions with three different ozone climatologies, including monthly averaged data from HALOE (HALogen Occultation Experiment), SAGE-II, and this ozone climatology for the 2000s (note that this climatology does not include ozonesonde data from 2010). For this initial experiment, rather than use the stratospheric and tropospheric climatologies separately, as suggested in Section 2.2, the complete stratosphere-troposphere climatology was used, with a dynamic adjustment of the ozone climatology to the model-predicted tropopause height, as employed by Makar et al. (2010). The ozone profiles from the three GEM-MACH global simulations were averaged from May 10 to June 20 and compared with independent ozonesondes for the same period at six CalNex campaign stations (Figure 16). Although modeled ozone for heights above 15 km are generally in good agreement, large discrepancies can be found in the UTLS region (8-15 km) between the ozonesondes and the simulations. Using the ozonesondes as reference, the simulated ozone profiles in the upper troposphere and over the UTLS region are generally improved in shape and magnitude when this climatology is used, compared to those using the satellite climatologies. The improvement appears best at Joshua Tree, Point Reyes, and Point Sur over 5-15 km, where HALOE and SAGE tends to overestimate and underestimate the ozone value, respectively. At Shasta, Trinidad Head, and Kelowna (all further north), the profiles are better in the troposphere with the new ozonesonde climatology, but in the UTLS all the model profiles are too smooth compared to the ozonesondes (black line), suggesting that there is dynamical activity in the UTLS that is not well-represented in the model, or that the use of single stratosphere-troposphere climatologies tends unduly to smooth the sharp change in mixing ratio at the tropopause.

6 Conclusions

A new ozone climatology (1960s-2000s) in 3 dimensions (latitude, longitude, and altitude) has been developed based on the global ozonesonde record and trajectory statistics. The input data comprise 51898 ozone soundings at 111 stations over 44 years (1965-2008), obtained from the WOUDC. Forward and backward trajectories are performed for 4 days each from each sounding, driven by NCEP reanalysis data. The resulting global ozone climatology is archived monthly for five decades from the 1960s to the 2000s with a grid size of 5°×5°×1 km (latitude, longitude, and altitude). The ozone climatology is also archived yearly from 1965 to 2008 at the same horizontal and vertical resolutions.

This climatology dataset is tested at 20 selected stations by comparing the actual ozone sounding profile with that derived through the trajectory technique, using the ozone soundings at all stations except the one being tested. The two sets of profiles are in good agreement with an overall correlation coefficient of 0.99 and an RMS error of 224 ppbv (Figure 3). By individual station, the correlation coefficient ranges between 0.975 and 0.998 and RMS error between 87 and 482 ppbv. The ozone climatology is also compared with two sets of satellite data, from SAGE and OSIRIS, in the stratosphere. Although agreement is generally quite good (within 10%), there are larger biases in the UTLS, especially over mountains and in areas where ozonesonde measurements are particularly sparse.

The comparison with ozonesondes and satellite measurements provides us some confidence that the trajectory-mapping approach is an effective tool for interpolating sparse ozonesonde measurements. The comparison also assesses where uncertainties and limitations lie. Overall, we have more confidence in this climatology over the northern hemisphere than over the southern hemisphere, and in the middle and high latitudes than in the tropics.

At the defined grid system of 5°×5°×1 km (latitude, longitude, altitude), there are enough samples to separate decadal and seasonal variations (Figures 12 and 13), especially after the

516 1990s when SHADOZ data became available. However, there are still gaps, about 25% after the
517 1990s and mainly over the tropical oceans, which are interpolated with a spherical function
518 smoothing algorithm (Figure 13).

519 The ozone climatology in the long-term mean (1970s-2000s) can capture the general
520 features in the ozone distribution, such as the sharp gradient of ozone in the vicinity of the
521 tropopause, the latitudinal variation of tropopause height, and the ozone gradient between low
522 and high latitudes (Figures 10 and 11). Seasonal variability of ozone in both hemispheres, as well
523 as in the Arctic and the Antarctic, is captured (Figure 13).

524 The ozone climatology shows clearly the depletion of ozone in the northern middle and
525 high latitudes from the 1970s to the 1990s and ozone recovery in the 2000s (Figure 15), implying
526 possible faster recovery of ozone in the region than predicted by most atmospheric models. This
527 is consistent with analyses of satellite data from TOMS and SBUV/2 by Weatherhead and
528 Andersen (2006) and from OMI by Ziemke and Chandra (2012). Our ozone data, however, are
529 from an independent source and a record that is twice as long as the satellite record.

530 This ozone climatology has been used as the initial and upper boundary conditions for a
531 simulation of tropospheric ozone using the operational chemical forecast model at Environment
532 Canada. The model performance is improved notably in the vicinity of the tropopause (Figure
533 16).

534 Since the 1990s, trajectory mapping of atmospheric species has been explored with some
535 success, suggesting that the assumptions and principles for this approach are valid. The degree of
536 success depends on the credibility of the driving winds and available measurements of the
537 species of interest. The results of this study can provide insight for trajectory mapping of other
538 species having similar or longer lifetime. In the future, this work can be improved by including

more ozone measurement from different platforms, such as MOZAIC and SAGE. Longer trajectories could be employed in the stratosphere, and possibly better-resolved wind fields.

This ozone climatology is latitudinally, longitudinally, and vertically resolved and it can reveal longitudinal variation in the stratosphere that two-dimensional ozone climatologies cannot show. It covers higher latitudes than current satellite data, and also a rather longer time period. As it is neither dependent on *a priori data* nor photochemical modeling, it provides independent information and insights that can supplement satellite data and model simulations and enhance our understanding of stratospheric ozone.

Acknowledgements

The global ozone sounding data were obtained from the World Ozone and Ultraviolet Radiation Data Center (http://www.woudc.org) operated by Environment Canada, Toronto, Ontario, Canada, under the auspices of the World Meteorological Organization. We thank many whose dedication makes such a dataset possible. The SAGE and OSIRIS teams are appreciated for their datasets for validation. We acknowledge the trajectory model HYSPLIT (Hybrid Single Particle Lagrangian Integrated Trajectory Model) from the NOAA Air Resources Laboratory (http://www.arl.noaa.gov/ready.html), driven by the NCEP/NCAR reanalysis data from the NOAA Physical Sciences Division (http://www.esrl.noaa.gov/psd/data/reanalysis/reanalysis.shtml). The first author is grateful to the Natural Sciences and Engineering Research Council of Canada (NSERC) and Environment Canada for a research fellowship.

560 **References**

561 Attmannspacher, A., and Dütsch, H. U.: International ozone sonde intercomparison at the
562 Observatory Hohenpeissenberg, Ber. Dtsch. Wetterdienstes, 120, 1-85, 1970.
563 Attmannspacher, A., and Dütsch, H. U.: Second international ozone sonde intercomparison at
564 the Observatory Hohenpeissenberg, Ber. Dtsch.Wetterdienstes, 157, 1-64, 1980.
565 Baldwin, M. P., and Dunkerton, T. J.: Stratospheric harbingers of anomalous weather regimes,
566 Science, 294, 581-584, 2001.
567 Côté, J., Gravel, S. , Méthot, A., Patoine, A., and Roch, M.: The operational CMC-MRB Global
568 Environmental Multiscale (GEM) model, part I: Design considerations and formulation, Mon.
569 Wea. Rev., 126(6), 1373-1395, 1998.
570 Cunnold D. M., et al.: Validation SAGEII ozone measurements, J. Geophy. Res. 94, 8447-8460,
571 1989.
572 Degenstein, D. A., Bourassa, A. E., Roth, C. Z., and Llewellyn, E. J.: Limb scatter ozone
573 retrieval from 10 to 60 km using a multiplicative algebraic reconstruction technique, Atmos.
574 Chem. Phys., 9, 6521–6529, doi:10.5194/acp-9-6521-2009, 2009.
575 Deshler, T., Mercer, J., Smit, H. G. J., Stuebi, R., Levrat, G., Johnson, B. J., Oltmans, S. J.,
576 Kivi, R., Thompson, A. M., Witte, J., Davies, J., Schmidlin, F. J., Brothers, G., and Sasaki T.:
577 Atmospheric comparison of electrochemical cell ozoneso ndes from different manufacturers,
578 and with different cathode solution strengths: The Balloon Experiment on Standards for
579 Ozonesondes, J. Geophys. Res., 113, D04307, doi:10.1029/2007JD008975, 2008.
580 Draxler, R. R., and Hess, G. D.: An overview of the HYSPLIT_4 modeling system for
581 trajectories, dispersion and deposition, Aust. Met. Mag., 47, 295–308, 1998.
582 Draxler, R., Stunder, B., Rolph, G., Stein, A., Taylor, A.: HYSPLIT_4 User's Guide, 2012.

583 Eyring, V., et al.: Multimodel projections of stratospheric ozone in the 21st century, J. Geophys.
584 Res., 112, D16303, doi:10.1029/2006JD008332, 2007.
585 Fioletov, V. E.: D. Ozone Climatology, Trends, and Substances that Control Ozone,
586 ATMOSPHERE-OCEAN 46, 39–67 doi:10.3137/ao.460103, 2008.
587 Fioletov, V. E., Tarasick, D. W., and Petropavlovskikh, I.: Estimating ozone variability and
588 instrument uncertainties from SBUV(/2), ozonesonde, Umkehr, and SAGE II measurements:
589 Short-term variations , J. Geophys. Res., 111, D02305, doi:10.1029/2005JD006340, 2006.
590 Fleagle, R. G. and Businger, J. A.: An Introduction to Atmospheric Physics, 2nd ed., Academic,
591 San Diego, Calif., 1980.
592 Forster, P. M, et al.: Evaluation of radiation scheme performance within chemistry climate
593 models, J. Geophys. Res., 116, D10302, doi:10.1029 / 2010JD015361, 2011.
594 Fortuin, J., and Kelder, H.: An ozone climatology based on ozonesonde and satellite
595 measurements, J. Geophys. Res., 103, 31,709-31,733, 1988.
596 Gillett, N.P., and Thompson, D. W. J.: Simulation of recent Southern Hemisphere climate
597 change, Science, 302, 273-275, 2003.
598 Hare, E. W., Carty, E. J., Fioletov, V., and Wardle, D. I.: User Guide to the WMO/GAW World
599 Ozone Data Centre, Version 3.0, Environment Canada, 2007.
600 Hassler, B., Bodeker, G. E., and Dameris, M.: Technical Note: A new global database of trace
601 gases and aerosols from multiple sources of high vertical resolution measurements, Atmos.
602 Chem. Phys., 8, 5403–5421, doi:10.5194/acp-8-5403-2008, 2008.
603 Hering, W. S. and Dütsch, H. U.: Comparison of chemiluminescent and electrochemical
604 ozonesonde observations, J. Geophys. Res., 70(22), 5483–5490,
605 doi:10.1029/JZ070i022p05483, 1985.

606 Holton, J. R., Haynes, P. H., Mclntyre, M. E., et al.: Stratosphere-troposphere exchange. Rev.
607 Geophys, 33(4): 403-439, 1995.
608 Jacob, D. J.: Introduction to Atmospheric Chemistry, Princeton University Press: Princeton, NJ,
609 1999.
610 Jones, A., Urban, J., Murtagh, D. P., Eriksson, P. S., Brohede, Haley, C., Degenstein,
611 D., Bourassa, A., von Savigny, C., Sonkaew, T., Rozanov, A., Bovensmann, H., and
612 Burrows, J.: Evolution of stratospheric ozone and water vapour time series studied with
613 satellite measurements, Atmos. Chem. Phys., 9, 6055-6075, 2009.
614 Kalnay, E., Kanamitsu, M., Kistler, R., Collins, W., Deaven, D., Gandin, L., et al.: The
615 NCEP/NCAR 40-year reanalysis project. Bulletin of the American Meteorological Society, 77,
616 437– 471, 1996.
617 Kent et al.: A model for the separation of cloud and aerosols in SAGEII occultation data, *J.*
618 *Geophys. Res.* 98, 20,725-20735,1993.
619 Kerr, J. B., Fast, H., McElroy, C. T., Oltmans, S. J., Lathrop, J. A., Kyro, E., Paukkunen, A.,
620 Claude, H., Köhler, U., Sreedharan, C. R., Takao, T., and Tsukagoshi, Y.: The 1991 WMO
621 international ozonesonde intercomparison at Vanscoy, Canada, Atmosphere-Ocean, 32, 685-
622 716, 1994.
623 Lamsal, L., Weber, M., Tellmann, S., and Burrows, J.: Ozone column classified climatology of
624 ozone and temperature profiles based on ozonesonde and satellite data, J. Geophys. Res., 109,
625 D20304, doi:10.1029/2004JD004680, 2004.
626 Liu, S., and Ridley, B.: Tropospheric Ozone, In Atmospheric Chemistry and Global Change,
627 edited by Brasseur, G. P., J. J. Orlando, G. S. Tyndall, pp. 645-686, Oxford University Press,
628 1999.

629 Liu, G, Tarasick, D. W., Fioletov, V. E., Sioris, C. E., and Rochon, Y. J.: Ozone correlation
630 lengths and measurement uncertainties from analysis of historical ozonesonde data in North
631 America and Europe, J. Geophys. Res., 114, D04112, doi:10.1029/2008JD010576, 2009.
632 Liu, G, Liu, J. J., Tarasick, D. W., Fioletov, V. E., Jin, J. J., Najafabadi, O., Liu, Xiong, and
633 Sioris, C.E.: A global tropospheric ozone climatology from trajectory-mapped ozone
634 soundings, submitted to Atmospheric Chemistry and Physics Discussion, 13, 11473–11507,
635 2013.
636 Llewellyn, E. et al.: The OSIRIS instrument on the Odin spacecraft, Can. J. Phys., 82, 411–422,
637 2004.
638 Makar, P. A., Gong, W., Mooney, C., Zhang, J., Davignon, D., Samaali, M., Moran, M. D., He,
639 H., Tarasick, D. W., Sills, D., and Chen, J.: Dynamic adjustment of climatological ozone
640 boundary conditions for air-quality forecasts, Atmos. Chem. Phys., 10, 8997-9015,
641 doi:10.5194/acp-10-8997-2010, 2010.
642 McCormick, M. P.; Zawodny, J. M., Veiga, R. E., Larsen, J. C., Wang, P. H.: An overview of
643 sage I and II ozone measurements, Planet. Space Sci. 37, 1567-1586, 1989.
644 McLinden, C. A., Tegtmeier, S., and Fioletov, V.: Technical Note: A SAGE-corrected SBUV
645 zonal-mean ozone data set, Atmos. Chem. Phys. 9, 7963-7972, 2009.
646 Morris, G. A., Gleason, J. F., Ziemke, J., and Schoebert, M. R.: Trajectory mapping: A tool for
647 validation of trace gas observations, J. Geophy. Res., 105(D14), 17,875–17,894, 2000.
648 Murtagh, D., Frisk, U., Merino, F., Ridal, M., Jonsson, A., Stegman, J., Witt, G., Eriksson, P.,
649 Jimenez, C., Megie, G., de la Noe, J., Ricaud, P., Baron, P., Pardo, J. R., Hauchcorne, A.,
650 Llewellyn, E. J., Degenstein, D. A., Gattinger, R. L., Lloyd, N. D., Evans, W. F. J., McDade,
651 I. C., Haley, C. S., Sioris, C., von Savigny, C., Solheim, B. H., McConnell, J. C., Strong, K.,

652 Richardson, E. H., Leppelmeier, G. W., Kyrola, E., Auvinen, H., and Oikarinen, L.: An
653 overview of the Odin atmospheric mission, Can. J. Phys., 80, 309–319, 2002.
654 Newman, P. A. and Schoeberl, M. R.: A reinterpretation of the data from the NASA
655 Stratosphere-Troposphere Exchange Project, Geophys. Res. Lett., 22(18), 2501–2504, 1995.
656 Randel, W. and Wu, F.: Cooling of the Arctic and Antarctic Polar stratospheres due to ozone
657 depletion, J. Climate, 12, 1467-1479, 1999.
658 Randel, W. and Wu, F.: A stratospheric ozone profile data set for 1979-2005: variability, trends,
659 and comparisons with column ozone data, J. Geophys. Res., 111, D06313,
660 dio:10.1029/2006JD007339, 2007.
661 Schoeberl, M. R., Ziemke, J. R., Bojkov, B., Livesey, N., Duncan, B., Strahan, S., and others: A
662 trajectory-based estimate of the tropospheric ozone column using the residual method, J.
663 Geophys. Res., 112, D24S49, doi:10.1029/2007JD008773, 2007.
664 Shepherd, T. G. and Jonsson, A. I.: On the attribution of stratospheric ozone and temperature
665 changes to changes in ozone-depleting substances and well-mixed greenhouse gases, Atmos.
666 Chem. Phys., 8,1435– 1444, 2008.
667 Smit, H. G. J., Sträter, W., Helten, M., Kley, D., Ciupa, D., Claude, H. J., Köhler, U., Hoegger,
668 B., Levrat, G., Johnson, B., Oltmans, S. J., Kerr, J. B., Tarasick, D. W., Davies, J., Shitamichi,
669 M., Srivastav, S. K., and Vialle, C.: JOSIE: The 1996 WMO international intercomparison of
670 ozonesondes under quasi-flight conditions in the environmental chamber at Jülich, in
671 Atmospheric Ozone: Proceedings of the Quadrennial O_3 Symposium, l'Aquila, Italy, edited by
672 R. D. Bojkov and G. Visconti, pp. 971-974, Parco Sci. e Tecnol. d'Abruzzo, Italy, 1996.
673 Smit, H. G. J., Straeter, W., Johnson, B., Oltmans, S., Davies, J., Tarasick, D. W., Hoegger, B.,
674 Stubi, R., Schmidlin, F., Northam, T., Thompson, A., Witte, J., Boyd I., and Posny, F.:
675 Assessment of the performance of ECC-ozonesondes under quasi-flight conditions in the

environmental simulation chamber: Insights from the Juelich Ozone Sonde Intercomparison Experiment (JOSIE), J. Geophys Res., 112, D19306, doi:10.1029/2006JD007308, 2007.

SPARC CCMVal, SPARC CCMVal Report on the Evaluation of Chemistry-Climate Models, V. Eyring, T. G. Shepherd, D. W. Waugh (Eds.), SPARC Report No. 5, WCRP-X, WMO/TD-No. X, 2010.

Stohl, A., James, P., Forster, C., and Spichtinger, N.: An extension of Measurement of Ozone and Water Vapour by Airbus-In-service aircraft (MOZAIC) ozone climatologies using trajectory statistics, J. Geophys. Res., 106, D21, 27,757-27,768, doi:10.1029/2001JD000749, 2001.

Stohl, A., Bonasoni, P., Cristofanelli, P., Collins, W., Feichter, J., Frank, A., Forster, C., Gerasopoulos, E., Gäggeler, H., James, P., Kentarchos, T., Kromp-Kolb, H., Krüger, B., Land, C., Meloen, J., Papayannis, A., Priller, A., Seibert, P., Sprenger, M., Roelofs, G. J., Scheel, H. E., Schnabel, C., Siegmund, P., Tobler, L., Trickl, T., Wernli, H., Wirth, V., Zanis, P., and Zerefos, C.: Stratosphere-troposphere exchange: a review, and what we have learned from STACCATO, J. Geophys. Res., 108(D12), 8516, doi:10.1029/2002JD002490, 2003.

Sutton, R. T., Maclean, H., Swinbank, R., O'Neill, A., and Taylor, F. W.: High-resolution stratospheric tracer fields estimated from satellite observations using Lagrangian trajectory calculations, J. Atmos. Sci., 51, 2995-3005, 2004.

Talbot, D.; Moran, M. D., Bouchet, V., Crevier, L.-P., Menard, S., Kallaur, A.: Development of a New Canadian Operational Air Quality Forecast Model. In Air Pollution Modeling and Its Application XIX; Borrego, C., Miranda, A.I., Eds.; Springer: Berlin, Germany, pp. 470–478, 2009.

Tarasick, D. W., Moran, M. D., Thompson, A. M., Carey-Smith, T., Rochon, Y., Bouchet, V. S., Gong, W., Makar, P. A., Stroud, C., Ménard, S., Crevier, L.-P., Cousineau, S., Pudykiewicz,

700 J. A., Kallaur, A., Moffet, R., Ménard, R., Robichaud, A., Cooper, O. R., Oltmans, S. J.,
701 Witte, J. C., Forbes, G., Johnson, B. J., Merrill, J., Moody, J. L., Morris, G., Newchurch, M.
702 J., Schmidlin, F. J., and Joseph, E.: Comparison of Canadian Air Quality Forecast Models
703 with tropospheric ozone profile measurements above mid-latitude north america during the
704 IONS/ICARTT campaign: evidence for stratospheric input, J. Geophys. Res.,
705 112, No. D12, D12S22, doi:10.1029/2006JD007782, 2007.
706 Tarasick, D. W., Jin, J. J., Fioletov, V. E., Liu, G., Tompson, A. M., Oltmans, S. J., Liu, J.,
707 Sioris, C. E., Liu, X., Cooper, O. R., Dann, T., and Thouret, V.: High-resolution tropospheric
708 ozone fields for INTEX and ARCTAS from IONS ozonesondes, J. Geophys. Res., 115,
709 D20301, doi:10.1029/2009JD012918, 2010.
710 Thompson, A. M., Witte, J. C., McPeters, R. D., Oltmans, S. J., Schmidlin, F. J., Logan, J. A.,
711 Fujiwara, M., Kirchhoff, V. W. J. H., Posny, F., Coetzee, G. J. R., Hoegger, B., Kawakami,
712 S., Ogawa, T., Johnson, B. J., Vömel, H., and Labow, G.: Southern Hemisphere Additional
713 Ozonesondes (SHADOZ) 1998-2000 tropical ozone climatology 1. Comparison with Total
714 Ozone Mapping Spectrometer (TOMS) and ground-based measurements, J. Geophys. Res.,
715 108, D2, 8238, doi: 10.1029/2001JD000967, 2003a.
716 Thompson, A. M., Witte, J. C., Oltmans, S. J., Schmidlin, F. J., Logan, J. A., Fujiwara, M.,
717 Kirchhoff, V. W. J. H., Posny, F., Coetzee, G. J. R., Hoegger, B., Kawakami, S., Ogawa, T.,
718 Fortuin, J. P. F., and Kelder, H. M.: Southern Hemisphere Additional Ozonesondes
719 (SHADOZ) 1998-2000 tropical ozone climatology 2. Tropospheric variability and the zonal
720 wave-one, J. Geophys. Res., 108, D2,8241, doi: 10.1029/2002JD002241, 2003b.
721 Thompson, A. M., Witte, J. C., Smit, H. G. J., Oltmans, S. J., Johnson, B. J., Kirchhoff, V. W. J.
722 H., and Schmidlin, F. J.: Southern Hemisphere Additional Ozonesondes (SHADOZ) 1998-
723 2004 tropical ozone climatology: 3. Instrumentation, station-to-station variability, and

724 evaluation with simulated flight profiles, J. Geophys. Res., 112, D03304,
725 doi:10.1029/2005JD007042, 2007.
726 von Savigny, C., Haley, C. S., Sioris, C. E., McDade, I. C., et al.: Stratospheric ozone profiles
727 retrieved from Limb scattered sunlight radiance spectra measured by the OSIRIS instrument
728 on the Odin satellite, Geophys. Res. Lett., 30, 1755, doi:10.1029/2002GL016401,2003.
729 Wang, H. J., Cunnold, D. M., Thomason, L. W., Zawodny, J. M., and Bodeker, G. E.:
730 Assessment of SAGE version 6.1 ozone data quality, J. Geophys. Res., 107, 4691, doi:
731 10.1029 / 2002JD002418, 2002.
732 Wang. L. and Waugh, D. W.: Chemistry-climate model simulations of recent trends in lower
733 stratospheric temperatures and stratospheric residual circulation. J. Geophys. Res., 117,
734 D09109, doi:10.1029/2011JD017130, 2012.
735 Wardle, D.I., Hare, E. W., Carty, E. J., and Fioletov, V. E.: The Guide to the WMO/GAW
736 World Ultraviolet Radiation Data Centre (WUDC) Version 5.1, Atmospheric Environment
737 Service, Environment Canada, 1998.
738 Waugh, D. W., Oman, L., Kawa, S. R., Stolarski, R. S., Pawson, S., Douglass, A. R., Newman,
739 P. A., and Nielsen J. E.: Impacts of climate change on stratospheric ozone recovery, Geophys.
740 Res. Lett., 36, L03805, doi:10.1029/2008GL036223, 2009.
741 Weatherhead, E. C. and Andersen, S. B.: The search for signs of recovery of the ozone layer,
742 Nature, 441, 39–45, doi:10.1038/nature04746, 2006.
743 WMO(World Meteorological Organization): Scientific Assessment of Ozone Depletion: 2002,
744 Global Ozone Research and Monitoring Project--Report No. 47, Geneva, Switzerland, 498 pp.,
745 2003.

746 WMO (World Meteorological Organization): Scientific Assessment of Ozone Depletion: 2006,
747 Global Ozone Research and Monitoring Project --Report No. 50, Geneva, Switzerland, 572
748 pp., 2007.
749 World Climate Research Programme: SPARC/IOC/GAW Assessment of Trends in the Vertical
750 Distribution of Ozone, Stratospheric Processes and Their Role in Climate, World Meteorol.
751 Organ. Global Ozone Res. Monit. Proj. Rep. 43, Geneva, Switzerland, 1998.
752 Ziemke, J. R., Chandra, S., and Bhartia, P. K.: A 25-year data record of atmospheric ozone from
753 TOMS Cloud Slicing: Implications for trends in stratospheric and tropospheric ozone, J.
754 Geophys. Res., 110, D15105, doi:10.1029/2004JD005687, 2005.
755 Ziemke, J. R., Chandra, S., Labow, G. J., Bhartia, P. K., Froidevaux, L., and Witte, J. C.: A
756 global climatology of tropospheric and stratospheric ozone derived from Aura OMI and MLS
757 measurements, Atmos. Chem. Phys., 11, 9237–9251, 2011.
758 Ziemke, J. R. and Chandra, S.: Development of a climate record of tropospheric and
759 stratospheric column ozone from satellite remote sensing: evidence of an early recovery of
760 global stratospheric ozone, Atmos. Chem. Phys., 12, 5737-5753, 2012.

761

762

763 **Table 1**. Ozonesonde stations, including each station's station ID number, geolocation, the
764 number of profiles used in this study, as well as measurement period.

Station ID	Station Name	Latitude (°)	Longitude (°)	Altitude (m)	Start Year	End Year	No. Profiles
255	Ainsworth	42.6	-100	789	1986	1986	7
229	Albrook	9	-79.6	66	1980	1980	20
18	Alert	82.5	-62.4	127	1987	2008	1068
111	Amundsen-Scott	-90	0	2820	1965	1987	272
348	Ankara	40	32.9	896	1994	2001	167
328	Ascension Island	-8	-14.4	91	1990	2005	415
199	Barrow	71.3	-156.6	11	1974	1974	3
104	Bedford	42.5	-71.3	80	1969	1971	77
181	Berlin	52.5	13.4	50	1966	1973	350
197	Biscarrosse/Sms	44.4	-1.2	18	1976	1983	359
67	Boulder	40.1	-105.3	1689	1979	1996	556
338	Bratts Lake	50.2	-104.7	592	2003	2008	229
329	Brazzaville	-4.3	15.3	314	1990	1992	82
394	Broadmeadows	-37.7	144.9	108	1999	2003	219
72	Byrd	-80	-119.5	1528	1965	1966	59
38	Cagliari	39.3	9.1	4	1968	1980	419
108	Canton Island	-2.8	-171.7	3	1965	1965	31
20	Caribou	46.9	-68	192	1981	1981	1
444	Cheju	33.5	126.5	300	2001	2001	13
224	Chilca	-12.5	-76.8	-1	1975	1975	3
138	Christchurch	-43.5	172.6	34	1965	1965	25
77	Churchill	58.8	-94.1	35	1973	2008	1431
198	Cold Lake	54.8	-110.1	702	1977	1981	66
236	Coolidge Field	17.3	-61.8	10	1976	1976	7
334	Cuiaba	-15.6	-56.1	990	1992	1992	21
450	Davis	-68.6	78	16	2003	2005	61
316	De Bilt	52.1	5.2	9.5	1994	2006	650

238	Denver	39.8	-104.9	1611	1977	1977	1
441	Easter Island	-27.2	-109.4	62	1995	1997	75
21	Edmonton	53.6	-114.1	766	1970	2008	1562
456	Egbert	44.2	-79.8	253	2003	2008	185
213	El Arenosillo	37.1	-6.7	41	1977	1983	20
335	Etosha Pan	-19.2	15.9	1100	1992	1992	16
315	Eureka	80	-86.2	310	1992	2008	1077
105	Fairbanks	64.8	-147.9	138	1965	1965	47
438	Fiji	-18.1	178.3	6	1997	2005	247
203	Ft. Sherman	9.3	-80	57	1977	1977	16
228	Gimli	50.6	-97.1	228	1980	1985	31
76	Goose Bay	53.3	-60.4	40	1965	2008	1774
237	Great Falls	47.5	-111.4	1118	1977	1977	4
40	Haute Provence	43.9	5.7	674	1981	1997	61
477	Heredia	10	-84.1	1176	2006	2006	69
109	Hilo	19.6	-155.1	11	1965	2001	679
99	Hohenpeissenberg	47.8	11	975	1966	2007	4147
344	Hong Kong	22.3	114.2	66	2000	2007	310
418	Huntsville	34.7	-86.6	196	1999	2003	160
303	Iqaluit	63.8	-68.6	20	1991	1992	30
437	Java	-7.6	112.7	50	1998	2006	264
265	Irene	-25.9	28.2	1524	1990	2006	346
336	Isfahan	32.5	51.4	1550	1999	2008	101
404	Jokioinen	60.8	23.5	103	1995	1998	99
439	Kaashidhoo	5	73.5	1	1999	1999	54
7	Kagoshima	31.6	130.6	157.5	1969	2005	841
457	Kelowna	49.9	-119.4	456	2003	2008	234
225	Kourou	5.3	-52.7	4	1974	1974	3
149	La Paz	-16.5	-68	3420	1965	1965	10
436	La Reunion Island	-21.1	55.5	24	1998	2006	232
256	Lauder	-45	169.7	370	1986	2006	1270

254	Laverton	-37.9	144.8	21	1984	1999	384
221	Legionowo	52.4	21	96	1979	2008	1404
43	Lerwick	60.1	-1.2	80	1992	2001	551
174	Lindenberg	52.2	14.1	112	1975	2008	2074
235	Long View	32.5	-94.8	103	1976	1976	2
29	Macquarie Island	-54.5	159	6	1994	2003	343
308	Madrid / Barajas	40.5	-3.7	650	1994	2008	489
400	Maitri	-70.5	11.5	223.5	1994	1998	94
448	Malindi	-3	40.2	-6	1999	2006	87
233	Marambio	-64.2	-56.6	196	1988	2006	348
466	Natal	-5.4	-35.3	32	2002	2007	177
227	Mcdonald Observatory	30.7	-90.9	2081	1969	1969	6
88	Mirny	-66.6	93	30	1989	1991	114
190	Naha	26.2	127.7	27	1989	2008	706
175	Nairobi	-1.3	36.8	1745	1996	2006	398
219	Natal	-5.9	-35.2	32	1979	2000	215
323	Neumayer	-70.7	-8.3	42	1992	2008	1198
10	New Delhi	28.5	77.2	247.5	1984	2006	146
280	Novolasarevskaya	-70.8	11.9	110	1985	1991	393
89	Ny Alesund	78.9	11.9	242.5	1990	2006	1541
210	Palestine	31.8	-95.7	121	1975	1985	163
156	Payerne	46.5	6.6	491	1968	2007	4776
217	Poker Flat	65.1	-147.5	357.5	1979	1982	40
187	Poona	18.6	73.9	559	1984	2003	112
333	Porto Nacional	-10.8	-48.4	240	1992	1992	15
242	Praha	50	14.5	304	1979	2008	1242
131	Puerto Montt	-41.5	-72.8	5	1965	1965	5
24	Resolute	74.7	-95	40	1966	2008	1649
297	S. Pietro Capofiume	44.7	11.6	11	1984	1993	98
191	Samoa	-14.3	-170.6	82	1995	2006	435
434	San Cristobal	-0.9	-89.6	8	1998	2006	271

239	San Diego	32.8	-117.2	72.5	1977	1977	2
234	San Juan	18.5	-66.1	17	1976	1976	6
401	Santa Cruz	28.4	-16.3	36	1996	2003	320
12	Sapporo	43.1	141.3	19	1969	2008	1004
443	Sepang Airport	2.7	101.7	17	1998	2007	235
132	Sofia	42.8	23.4	588	1982	1991	239
231	Spokane	47.7	-117.4	576	1976	1976	7
101	Syowa	-69	39.6	22	1966	2008	1284
432	Tahiti	-18	-149	2	1995	1999	168
95	Taipei	25	121.5	25	2000	2001	64
14	Tateno / Tsukuba	36.1	140.1	31	1968	2008	1299
157	Thalwil	46.8	8.5	515	1966	1968	183
205	Thiruvananthapuram	8.5	77	60	1984	2006	165
460	Thule	76.5	-68.7	57	1991	2003	248
65	Toronto	43.8	-79.5	198	1976	1994	16
445	Trinidad Head	40.8	-124.2	55	1999	2001	109
53	Uccle	50.8	4.4	100	1965	2007	4648
318	Valentia	51.9	-10.3	14	1994	2008	352
257	Vanscoy	52.1	-107.2	510	1990	2004	57
107	Wallops Island	37.9	-75.5	13	1970	2008	1280
64	Washington	39	-77.5	84	1965	1966	89
194	Yorkton	51.3	-102.5	504	1975	1978	72

768 **Table 2**. Geolocation of the 20 stations for validation.

Station ID	Station Name	Latitude (º)	Longitude (º)	Altitude (m)
328	Ascension Island	-8	-14.4	91
67	Boulder	40.1	-105.3	1689
315	Eureka	80	-86.2	310
438	Fiji	-18.1	178.3	6
76	Goose Bay	53.3	-60.4	40
109	Hilo	19.6	-155.1	11
99	Hohenpeissenberg	47.8	11	975
344	Hong Kong	22.3	114.2	66
265	Irene	-25.9	28.2	1524
336	Isfahan	32.5	51.4	1550
256	Lauder	-45	169.7	370
190	Naha	26.2	127.7	27
175	Nairobi	-1.3	36.8	1745
219	Natal	-5.9	-35.2	32
323	Neumayer	-70.7	-8.3	42
191	Samoa	-14.3	-170.6	82
434	San Cristobal	-0.9	-89.6	8
401	Santa Cruz	28.4	-16.3	36
432	Tahiti	-18	-149	2
53	Uccle	50.8	4.4	100

769

770

Table 3. Comparison of the ozone climatology and SAGE in the 1990s and the 2000s at three altitudes in NH winter (DJF) and summer (JJA), respectively. All the correlation coefficients (*r*) are significant at a significance level <1% ($p<0.01$). $O_{3(Clim)}$ and $O_{3(SAGE)}$ are the ozone mixing ratios for the climatology and SAGE data, respectively, averaged over grid cells where both data are available (the number of grid cells is indicated as *N*). RMS is the root mean square difference between the climatology and SAGE data; and RMS/Mean is the ratio of the RMS to the mean of $O_{3(Clim)}$ and $O_{3(SAGE)}$.

Variables	14.5 km		19.5 km		24.5 km	
	DJF	JJA	DJF	JJA	DJF	JJA
	1990s					
$O_{3(Clim)}$ (ppbv)	328	313	1736	1584	4763	4677
$O_{3(SAGE)}$ (ppbv)	312	286	1747	1640	4632	4711
$O_{3(Clim)}$/ $O_{3(SAGE)}$	1.05	1.09	0.99	0.97	1.03	0.99
RMS (ppbv)	104	87	413	337	714	508
RMS/Mean (%)	33	29	24	21	15	11
r	0.94	0.95	0.85	0.86	0.31	0.62
N	1967	1908	1633	1544	1636	1579
	2000s					
$O_{3(Clim)}$ (ppbv)	323	310	1698	1580	4950	4817
$O_{3(SAGE)}$ (ppbv)	306	286	1702	1624	4651	4737
$O_{3(Clim)}$/ $O_{3(SAGE)}$	1.06	1.08	1.00	0.97	1.06	1.02
RMS (ppbv)	116	105	405	337	819	679
RMS/Mean (%)	37	35	24	21	17	14
r	0.93	0.92	0.87	0.87	0.32	0.46
N	1930	1904	1630	1496	1584	1618

781 **Table 4**. Decadal variability of ozone mixing ratio at 19.5 km averaged over the globe, the
782 Arctic (60-90° N), and the Antarctic (60-90° S) from the 1970s to the 2000s in January and July.
783 The mean is area-weighted and is computed taking only values from grid cells where ozone data
784 are available in all four decades. The change is relative to the mean in %.

	The Globe		The Arctic		The Antarctic	
Decade	Ozone (ppbv)	Change (%)	Ozone (ppbv)	Change (%)	Ozone (ppbv)	Change (%)
	January					
1970s	2665	8.0	3578	9.8	2772	2.9
1980s	2534	2.7	3308	1.5	2753	2.2
1990s	2297	-6.9	3044	-6.6	2592	-3.8
2000s	2375	-3.8	3108	-4.6	2656	-1.4
Mean	2468		3260		2693	
	July					
1970s	2066	8.8	2364	7.6	3519	7.6
1980s	1905	0.3	2179	-0.9	3323	1.7
1990s	1820	-4.2	2085	-5.2	3096	-5.3
2000s	1805	-4.9	2164	-1.5	3137	-4.0
Mean	1899		2198		3269	

785
786

787 **Table 5.** Standard error of the mean (SE/mean, in %), coverage (in % of the total grid cells), and
788 the number of samples per grid (in N/grid) by decade at 19.5 and 24.5 km, respectively.
789

	19.5 km			24.5 km		
Decade	SE/Mean (%)	Coverage (%)	N/grid	SE/Mean (%)	Coverage (%)	N/grid
1970s	6.3	33.5	20	3.9	30	22
1980s	7.1	51.7	18	5.0	46.1	19
1990s	6.1	74.3	26	3.9	72.8	26
2000s	6.4	72.4	23	4.0	72.8	22

790

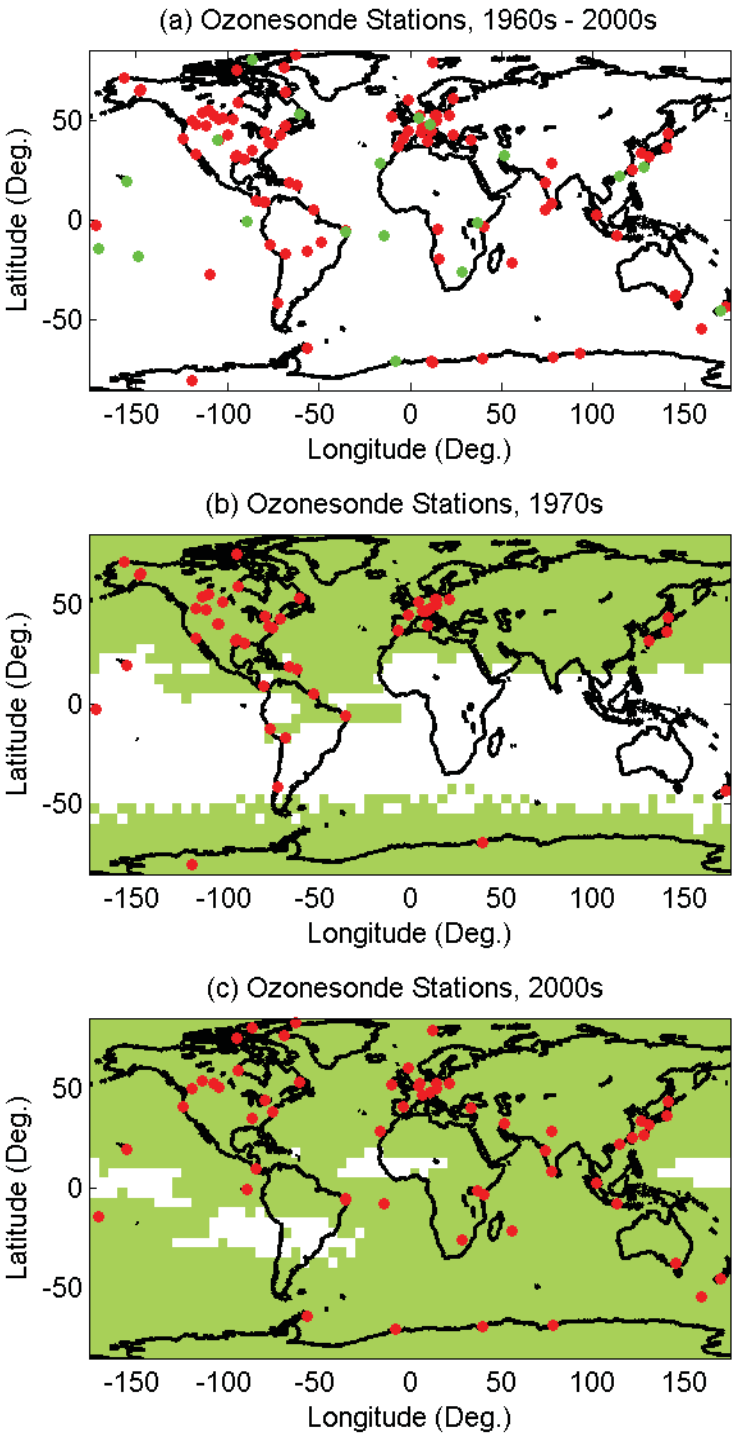

Fig. 1. Global distribution of ozonesonde stations (green and red dots) used in this study: (a) all stations from the 1960s to the 2000s, (b) in the 1970s, and (c) in the 2000s. Green dots in (a) indicate stations used for validation (see Table 2). In (b) and (c), the station locations are overlaid with the coverage of ozone climatology (in green) generated in this study at 19.5 km in the 1970s and the 2000s, respectively (see Figure 12 for the ozone values).

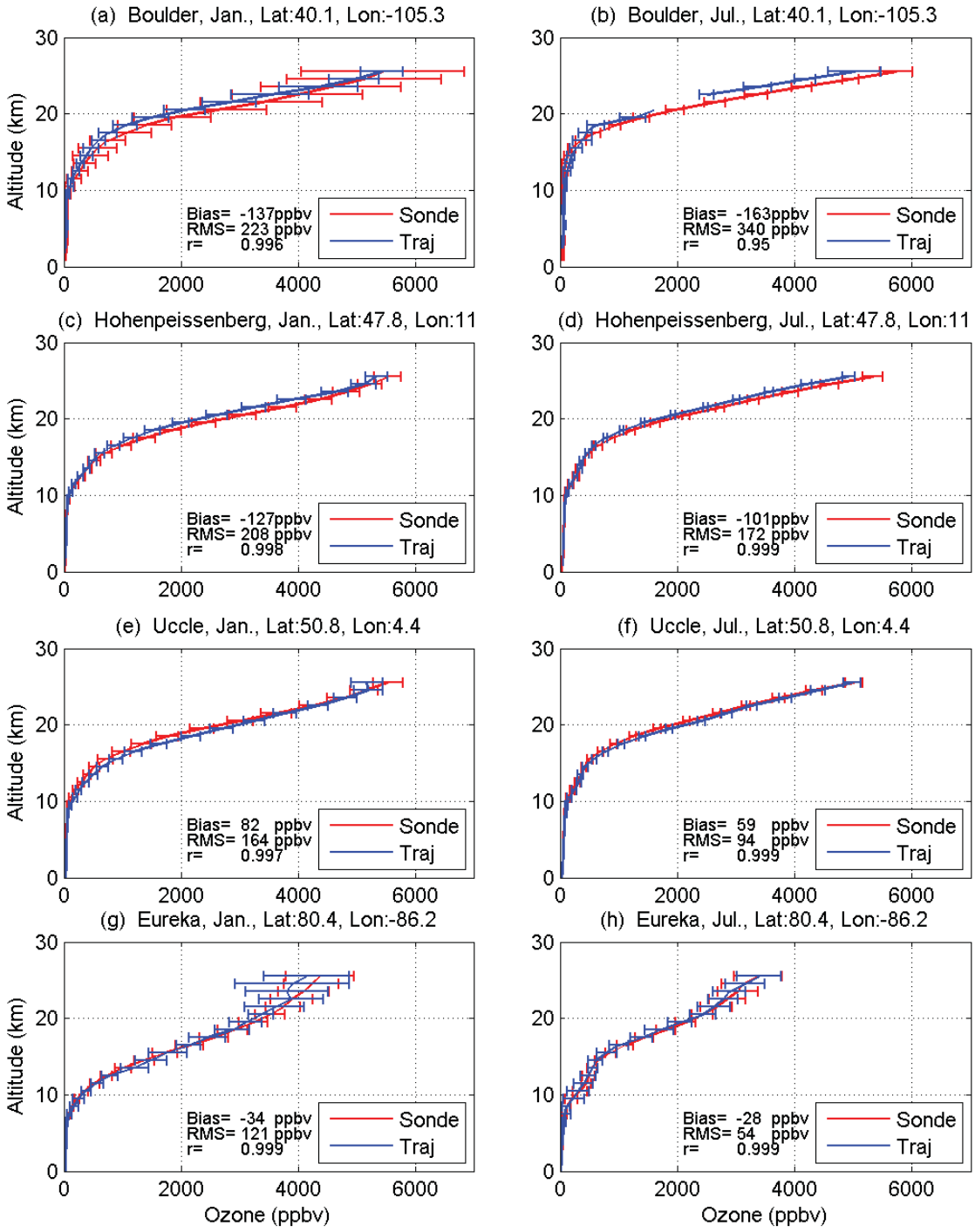

Fig. 2. Ozone profiles at Boulder, Hohenpeissenberg, Uccle, and Eureka: decadal monthly means in January (left panels) and July (right panels) in the 1990s. The actual sounding profiles are labeled as Sonde, while the profiles from trajectories without input from the station being tested are labeled as Traj. The error bar is 4 times the standard error of the mean (equivalent to 95% confidence limits on the averages).

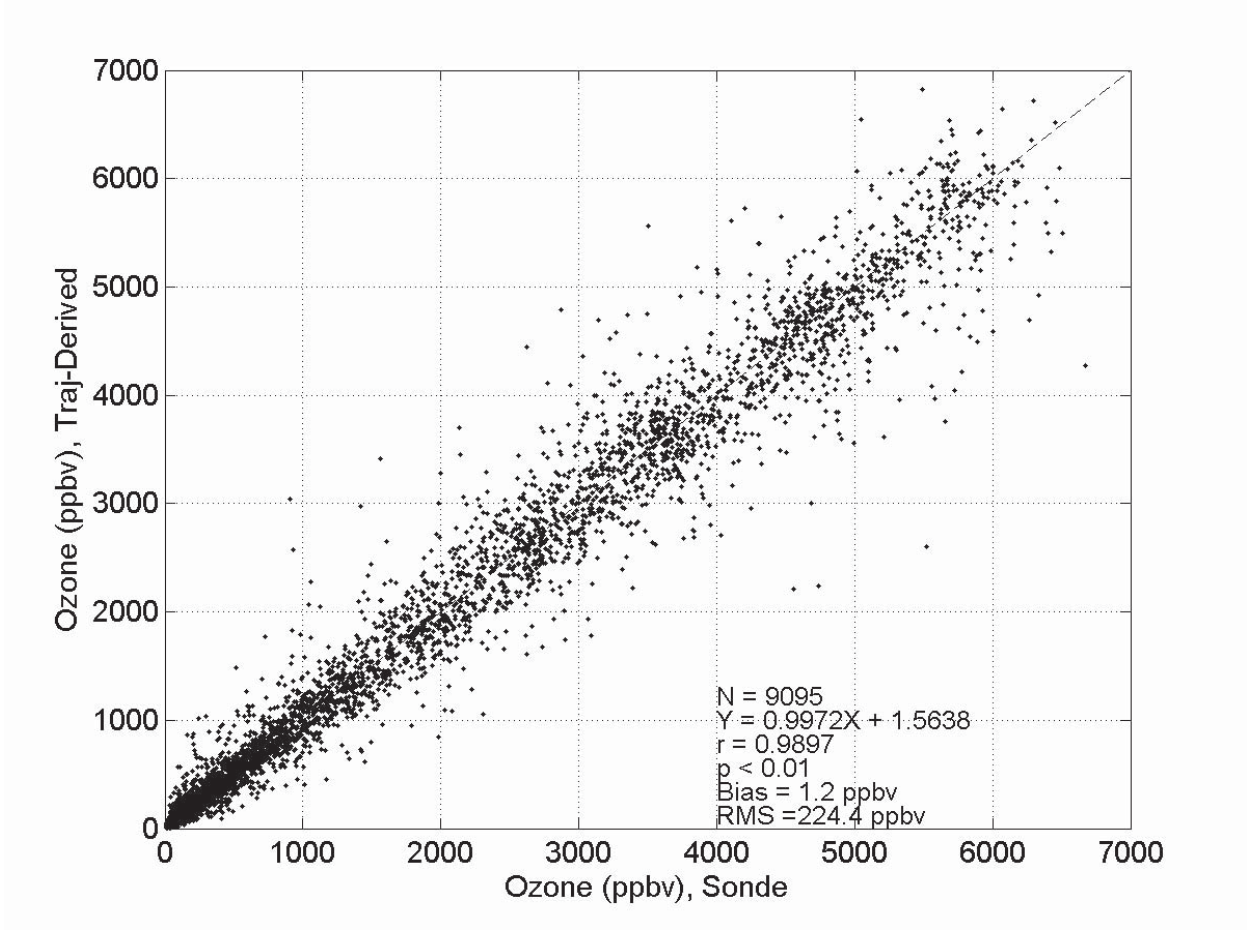

Fig. 3. Correlation (*r*) between ozone mixing ratios from ozonesondes and from trajectories, without input of the stations being tested, for 20 stations in the 1990s and the 2000s. The dashed line shows the 1:1 axis. The correlation is significant at the 1% level ($p<0.01$). *N* denotes the number of data points and RMS the root mean square error. *Y* represents trajectory-derived ozone mixing ratio and *X* ozone mixing ratio from ozonesondes.

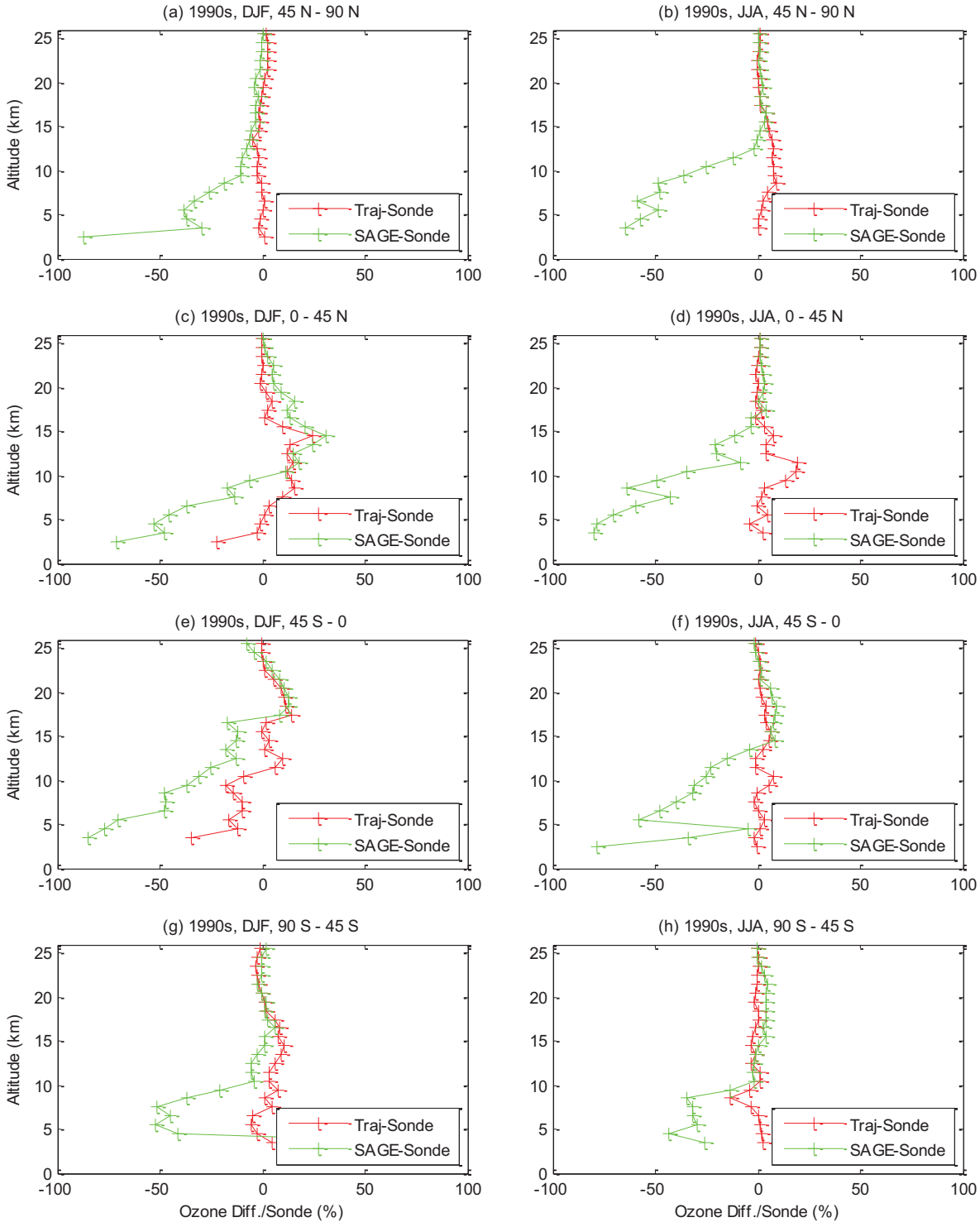

Fig. 4. Mean relative difference between the trajectory-derived ozone climatology and ozonesonde data (in red) for latitude zones 45–90° N, 0°–45° N, 45° S–0°, and 90–45° S in NH winter (DJF, left panels) and summer (JJA, right panels) in the 1990s. Coincident SAGE and ozonesonde profiles are compared in green. See text for details.

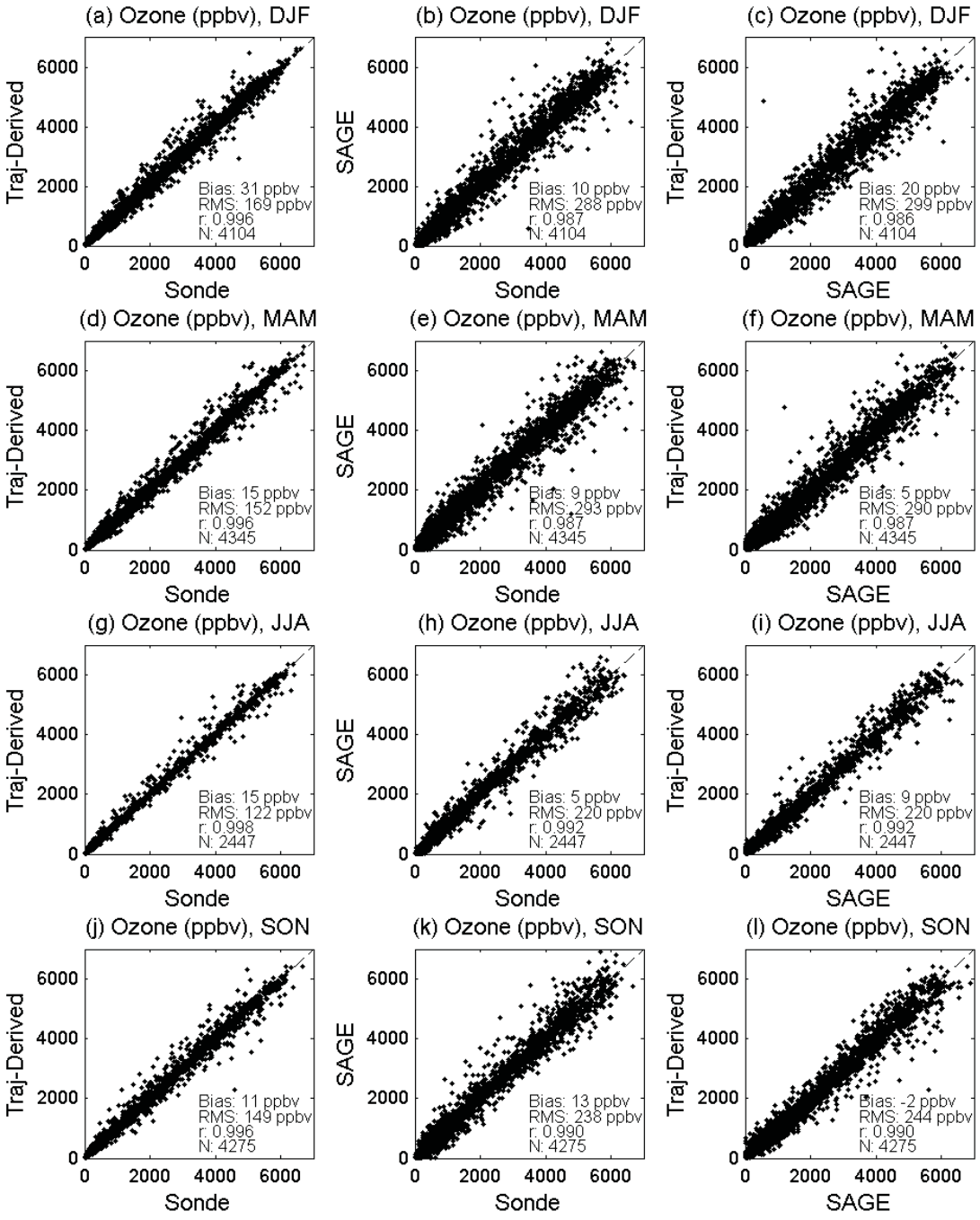

Fig. 5. Correlation (*r*) of ozone mixing ratio between trajectory-derived, SAGE, and ozonesonde data for the 1990s and 2000s for NH winter (1st row), spring (2nd row), summer (3rd row), and winter (4th row). The dashed line shows the 1:1 axis. *N* denotes the number of data points and RMS the root mean square error. All correlations are significant at a level better than 1%.

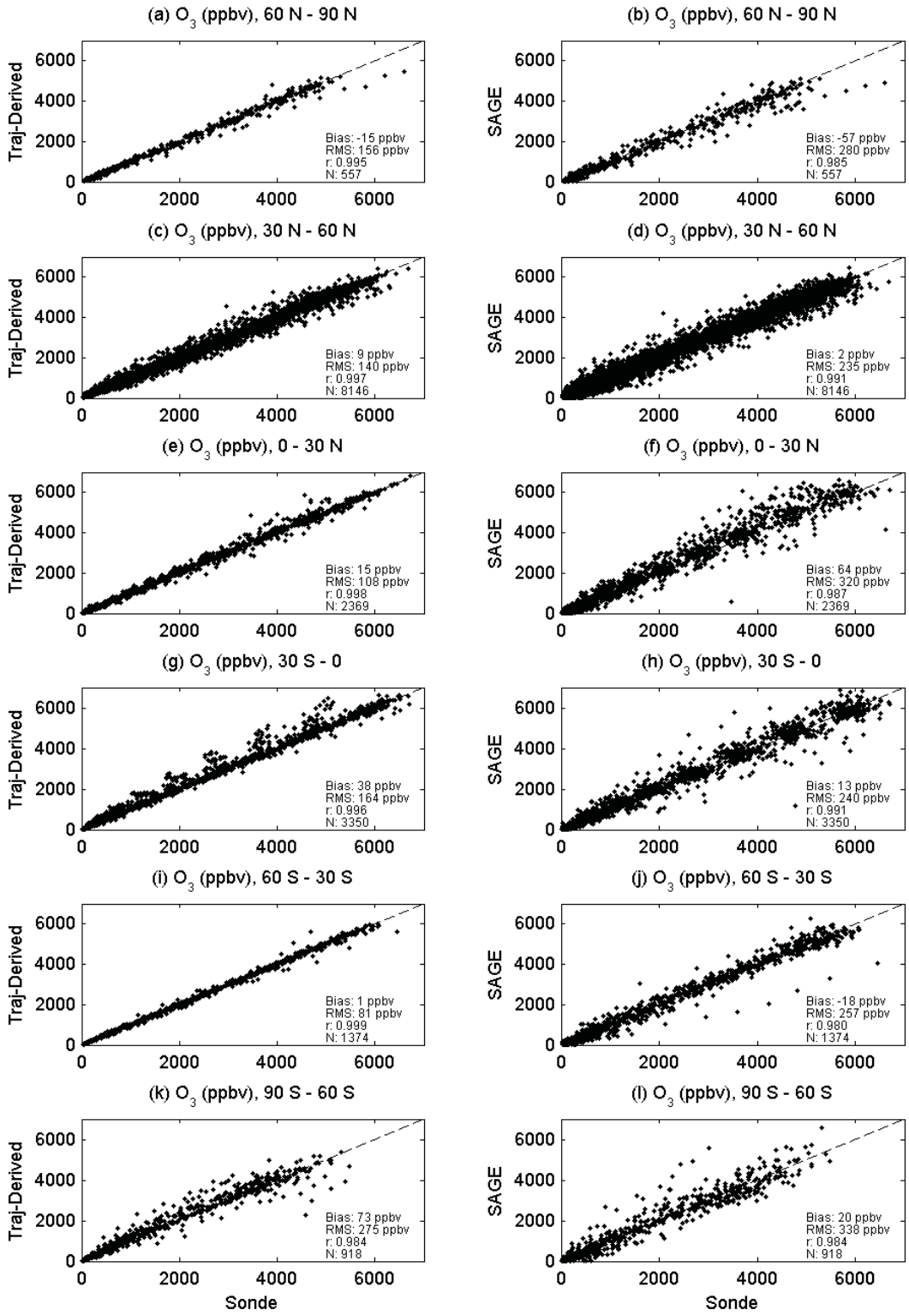

Fig. 6. Correlation (*r*) of ozone mixing ratio between trajectory-derived and ozonesonde data (left panels) and between SAGE and ozonesonde data (right panels) for the 1990s and 2000s for different latitude zones. The dashed line shows the 1:1 axis. *N* denotes the number of data points and RMS the root mean square error. All correlations are significant at a level better than 1%.

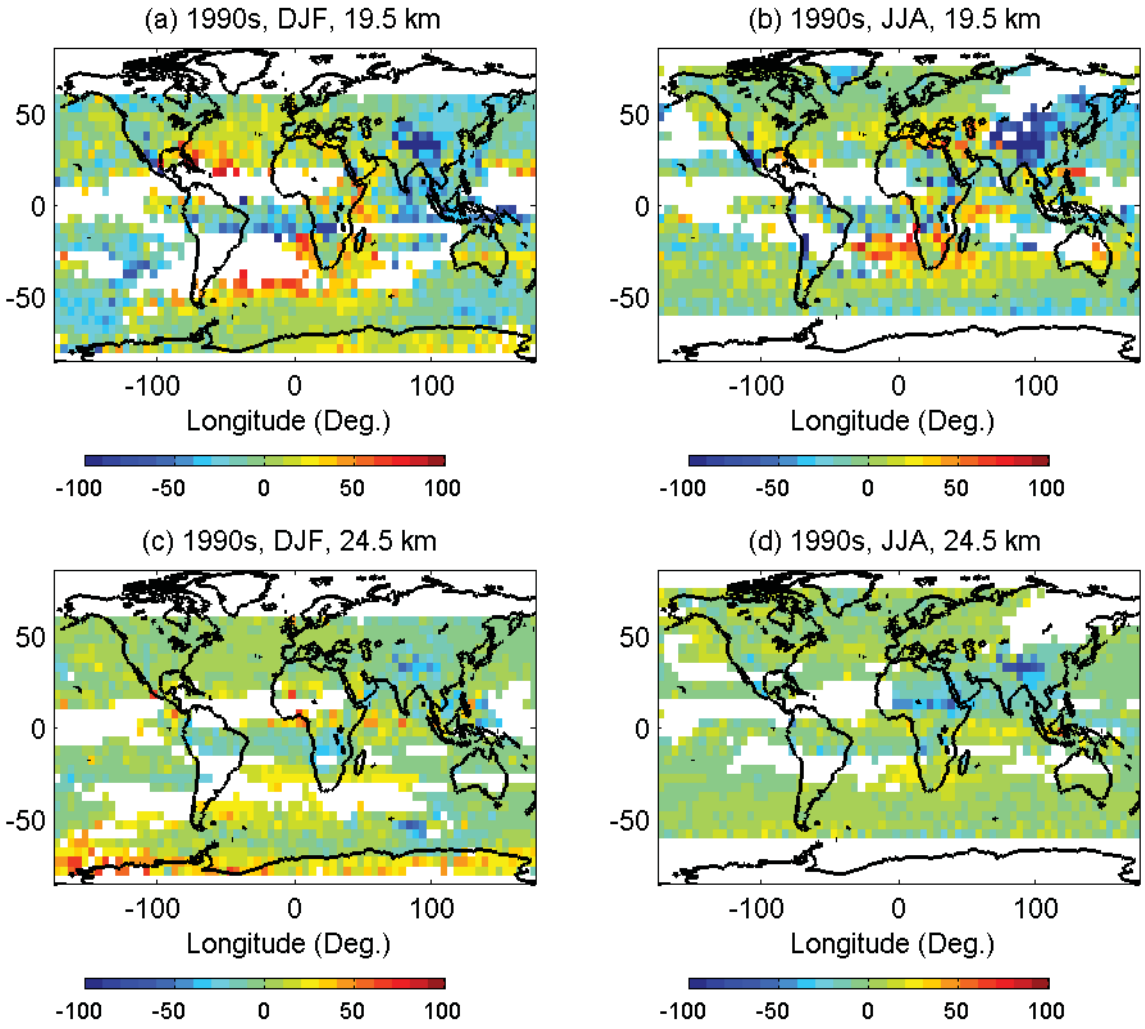

Fig. 7. Relative difference in ozone mixing ratio between the ozone climatology and SAGE data in NH winter (DJF, left panels) and summer (JJA, right panels) in the 1990s at 19.5 km (upper panels) and 24.5 km (lower panels). The comparison is made when both datasets are available at a cell and is expressed as the percentage difference of climatology minus SAGE divided by their mean.

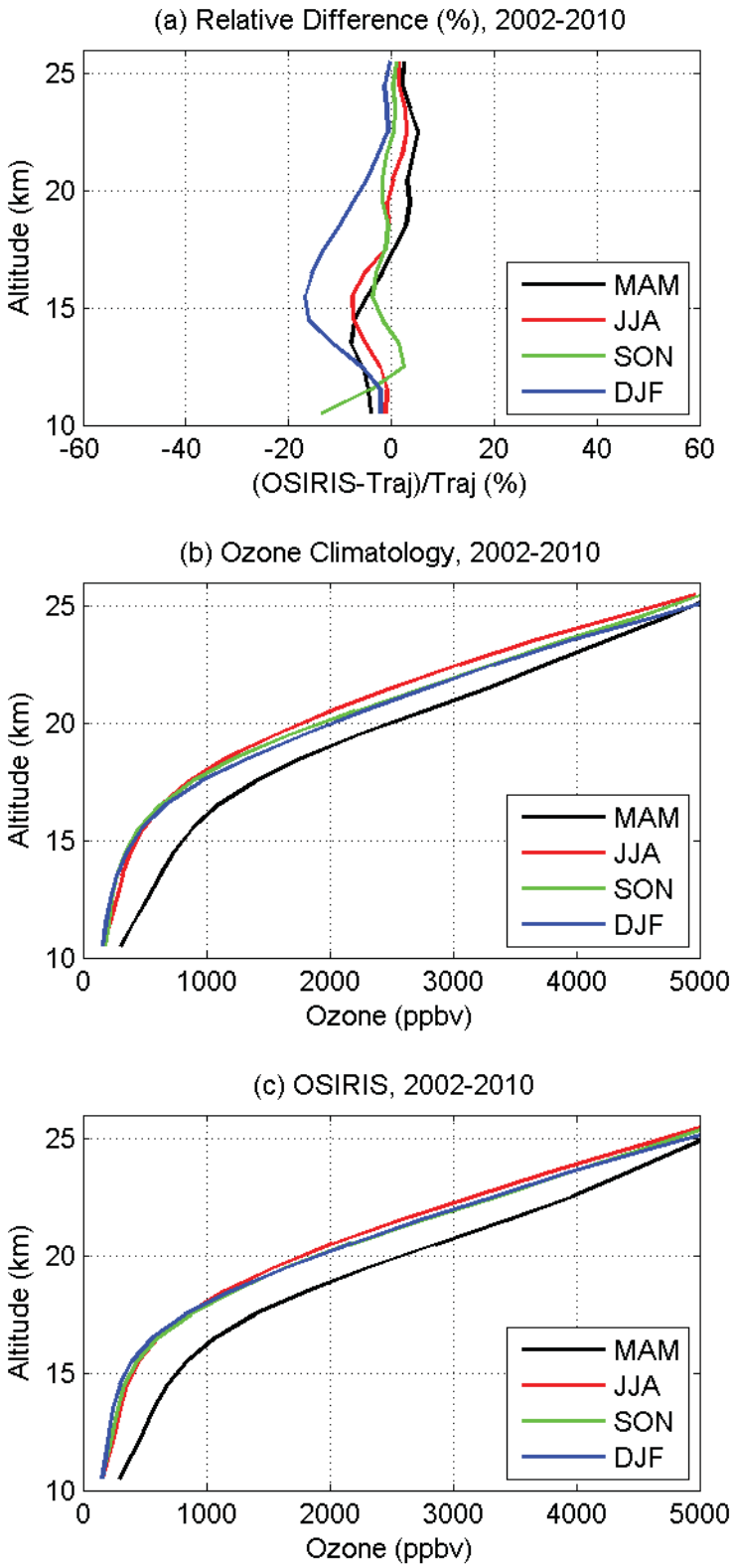

Fig. 8. (a) Altitude variation in relative difference between the trajectory-derived ozone climatology and OSIRIS data in four seasons, (b) Global mean ozone profile from the ozone climatology by season. (c) Global mean ozone profile from OSIRIS by season (NH spring: MAM, summer: JJA, fall: SON, winter: DJF).

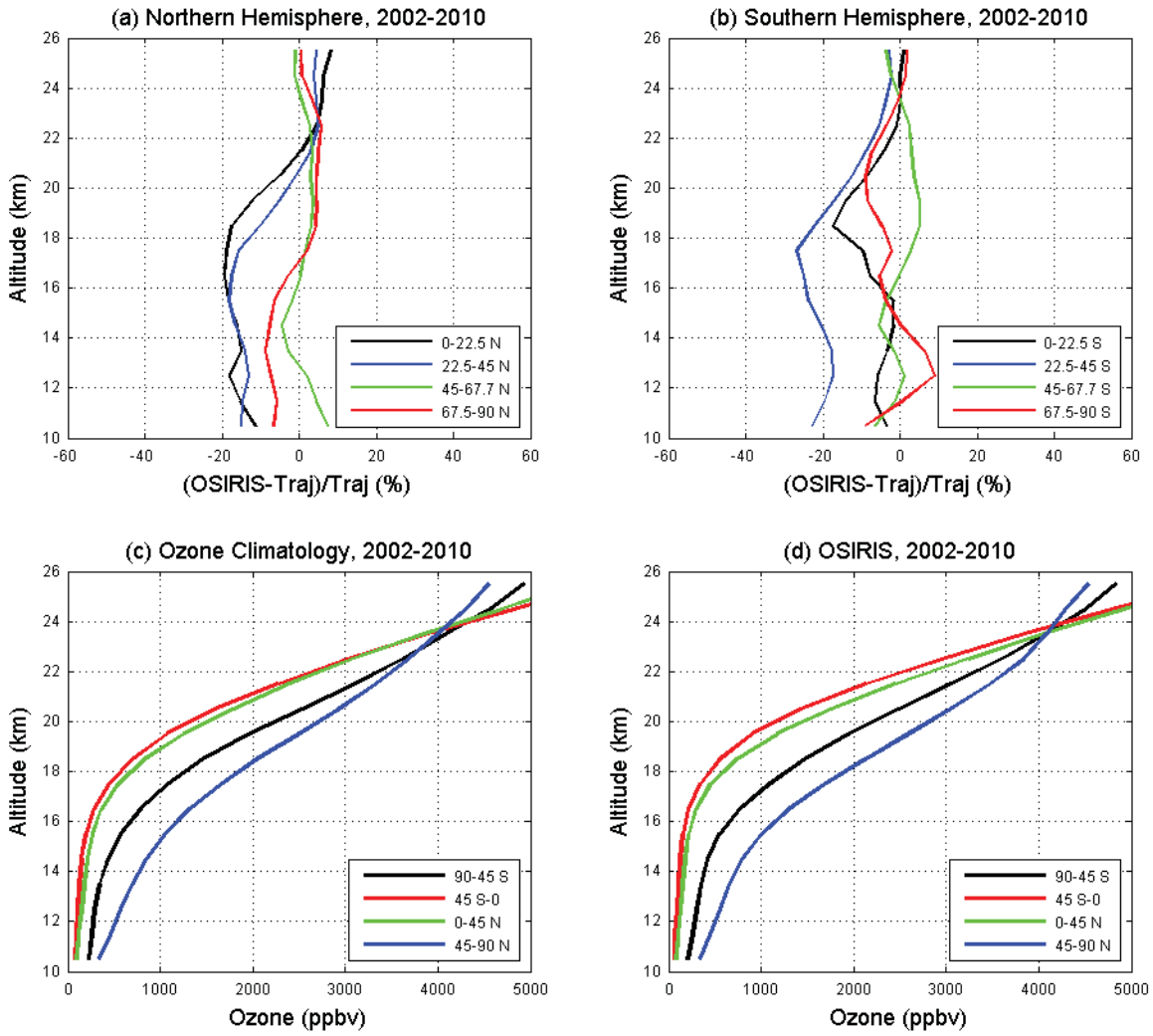

Fig. 9. Relative difference between the trajectory-derived ozone climatology and OSIRIS data in four latitude zones (a) in the northern hemisphere and (b) in the southern hemisphere, (c) global mean ozone profile from the ozone climatology in four latitude zones: 90-45° S, 45° S-0°, 0°-45° N, and 45-90° N, and (d) global mean ozone profile from OSIRIS in the four zones.

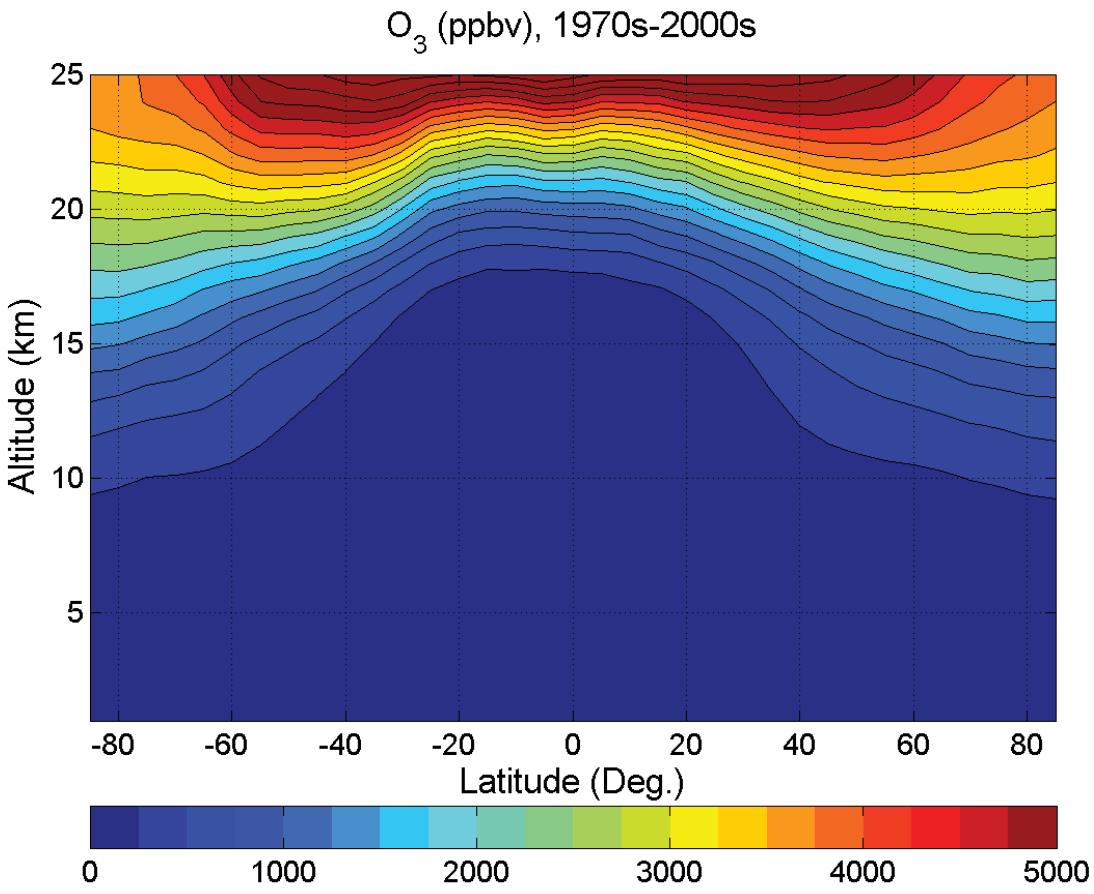

Fig. 10. Long-term latitude-altitude distribution of the ozone climatology (1970s-2000s).

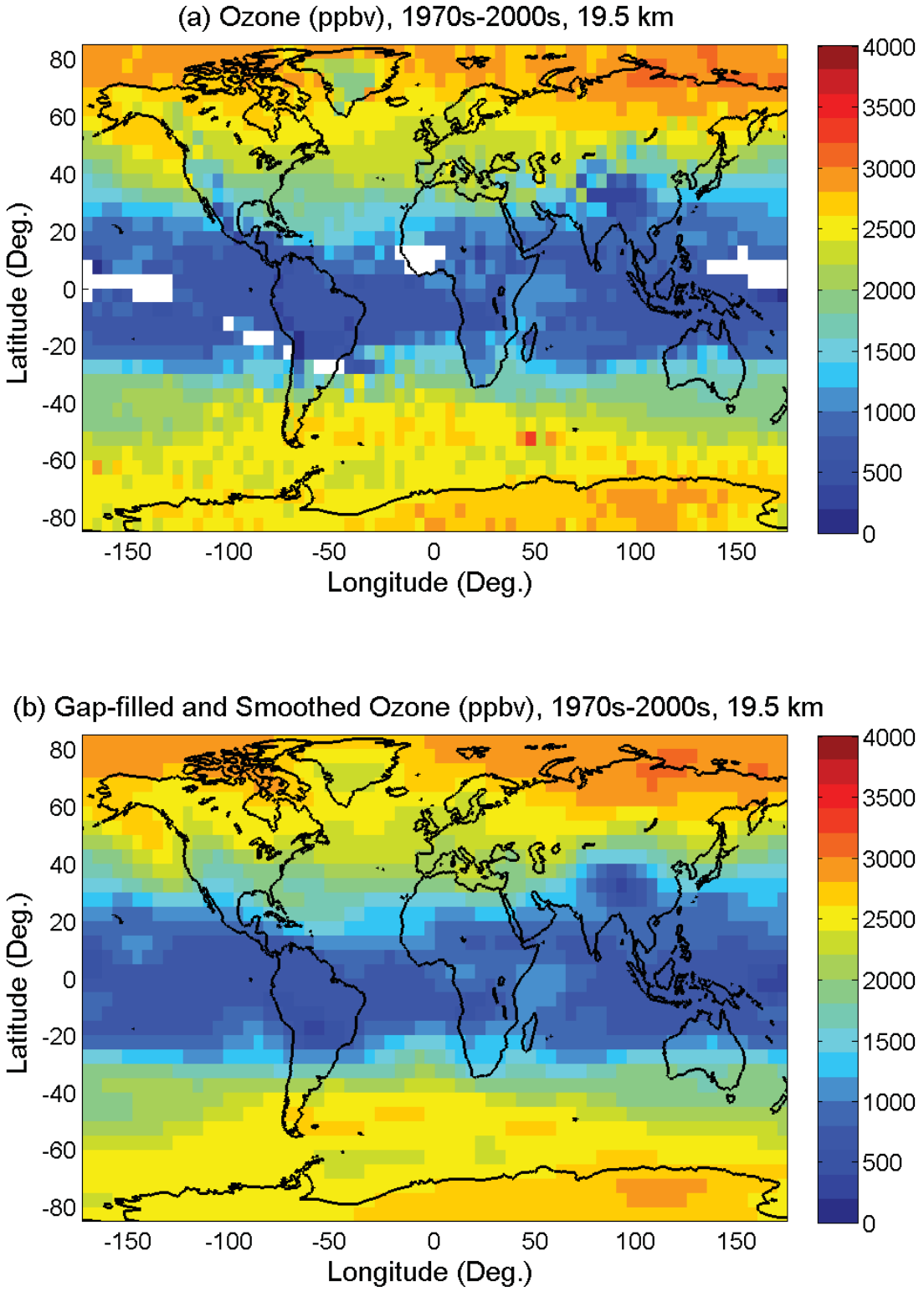

Fig. 11. (a) Long-term ozone climatology (1970s-2000s) at 19.5 km with gaps (white areas). (b) The gaps are filled and the ozone field is smoothed by a spherical function-based interpolation.

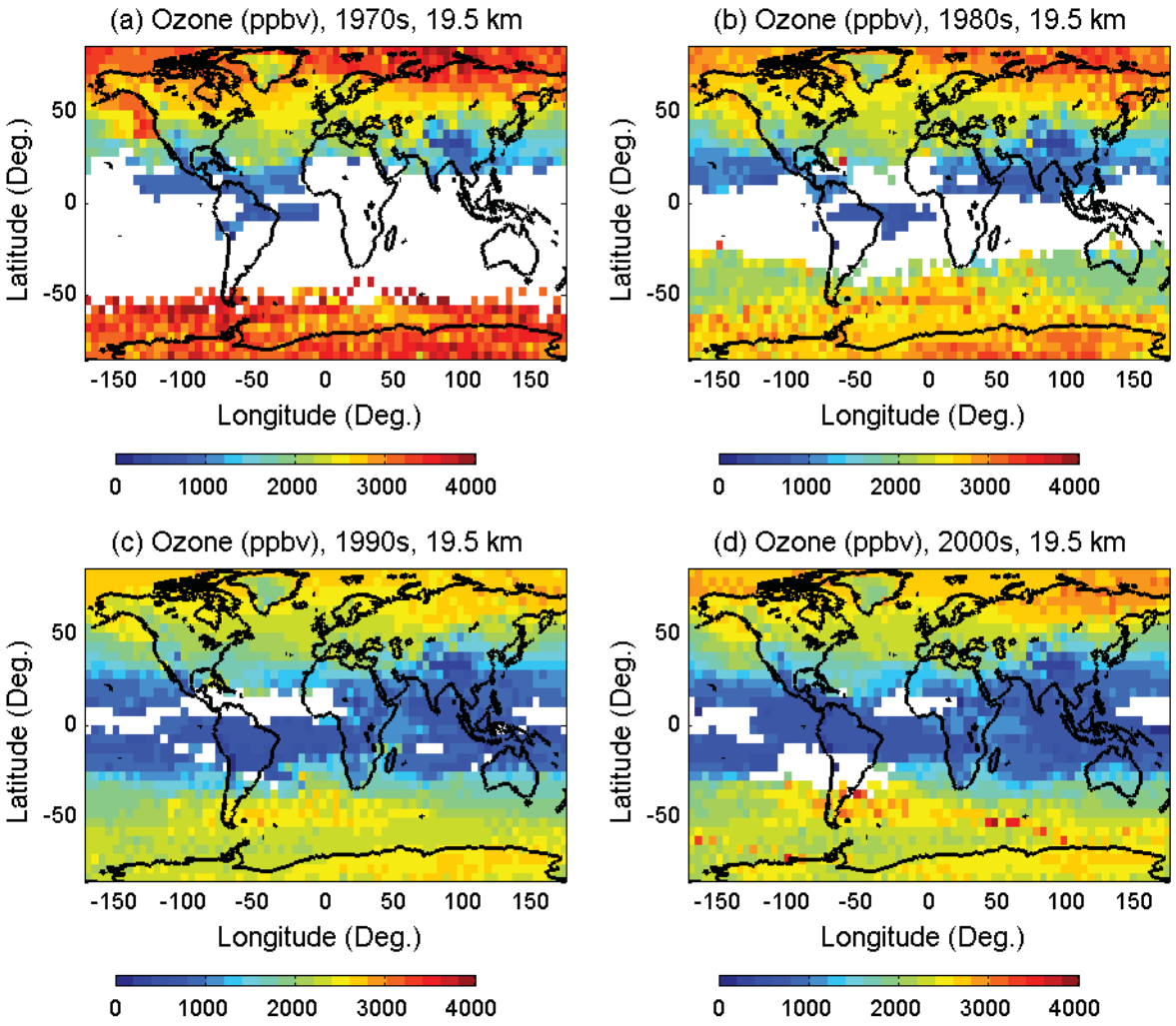

Fig. 12. Decadal variation in ozone at 19.5 km for (a) the1970s, (b) the 1980s, (c) the 1990s and (d) the 2000s. White areas indicate missing data.

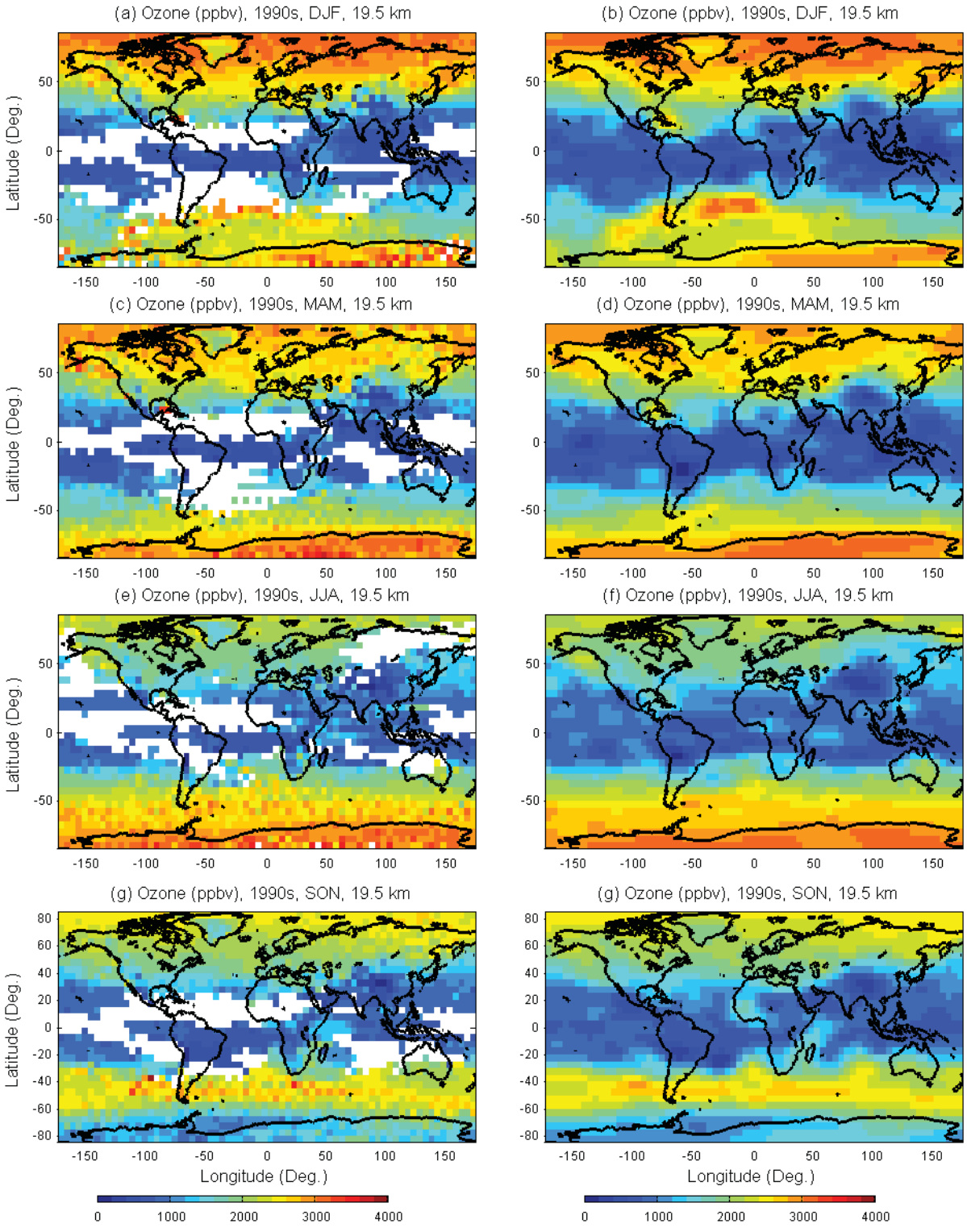

Fig. 13. Ozone fields with gaps (white areas) in the NH winter (DJF), spring (MAM), summer (JJA), and fall (SON) at 19.5 km in the 1990s (left panels) and the corresponding smoothed ozone fields (right panels).

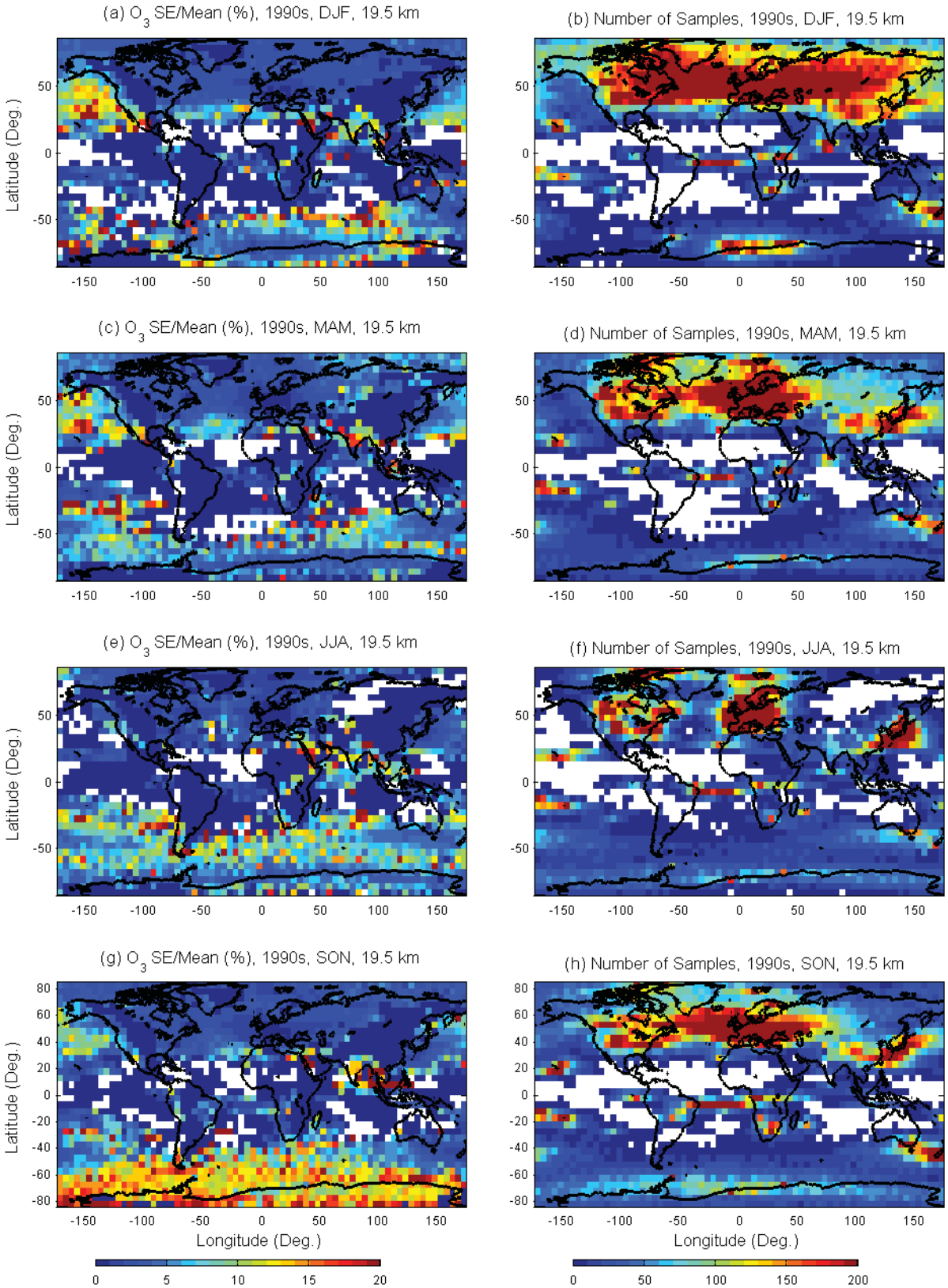

Fig. 14. The standard error of the mean (left panels) and number of samples (right panels) in the NH winter (DJF), spring (MAM), summer (JJA), and fall (SON) in the 1990s at 19.5 km.

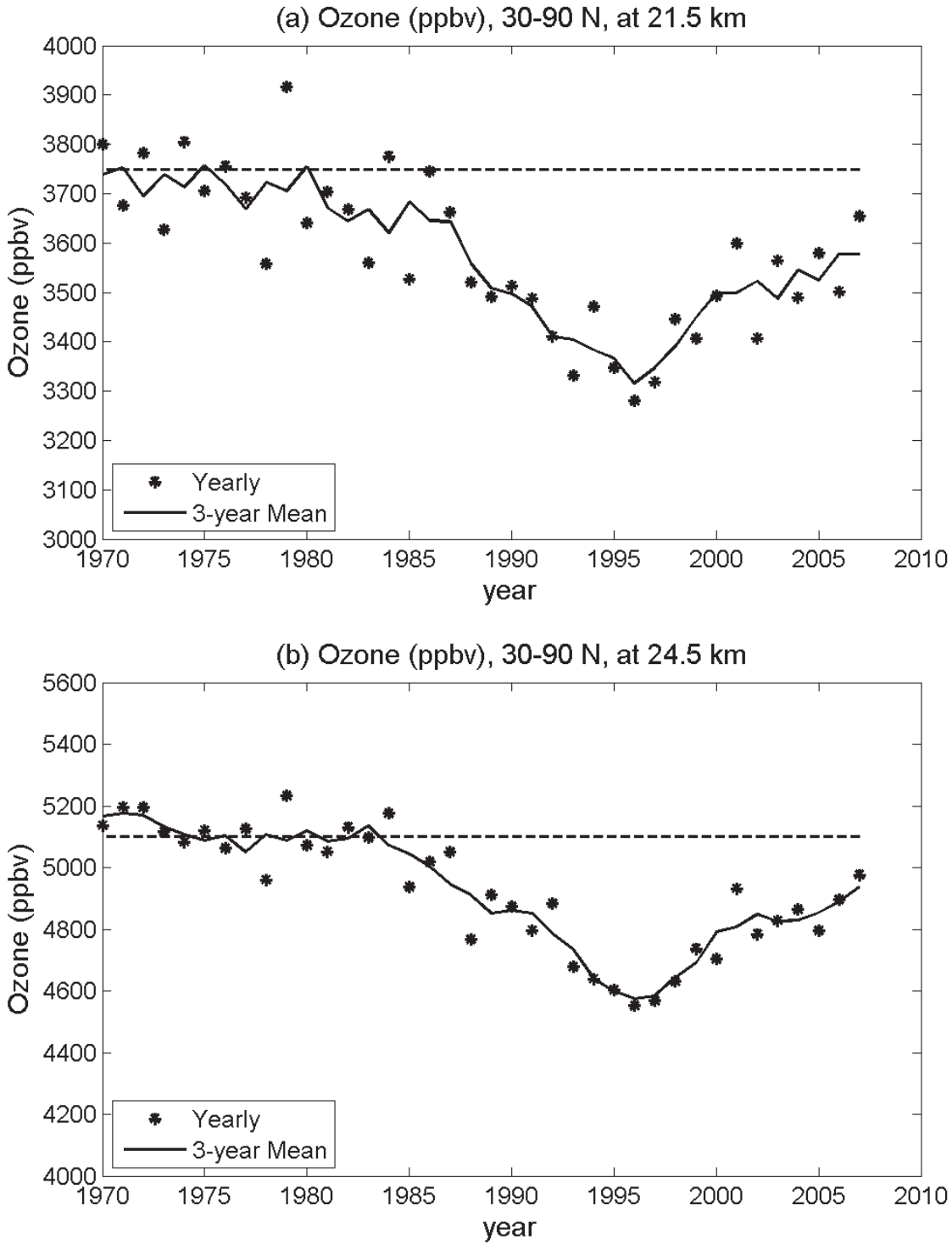

Fig. 15. Annual mean time series at (a) 21.5 km (~50 hPa) and (b) 24.5 km (~40 hPa) averaged over 30-60°N. The solid line is a 3-year running mean and the dashed line indicates the average ozone level before 1980. The area-weighted average is taken using data only from the grid cells where ozone data are available in all years.

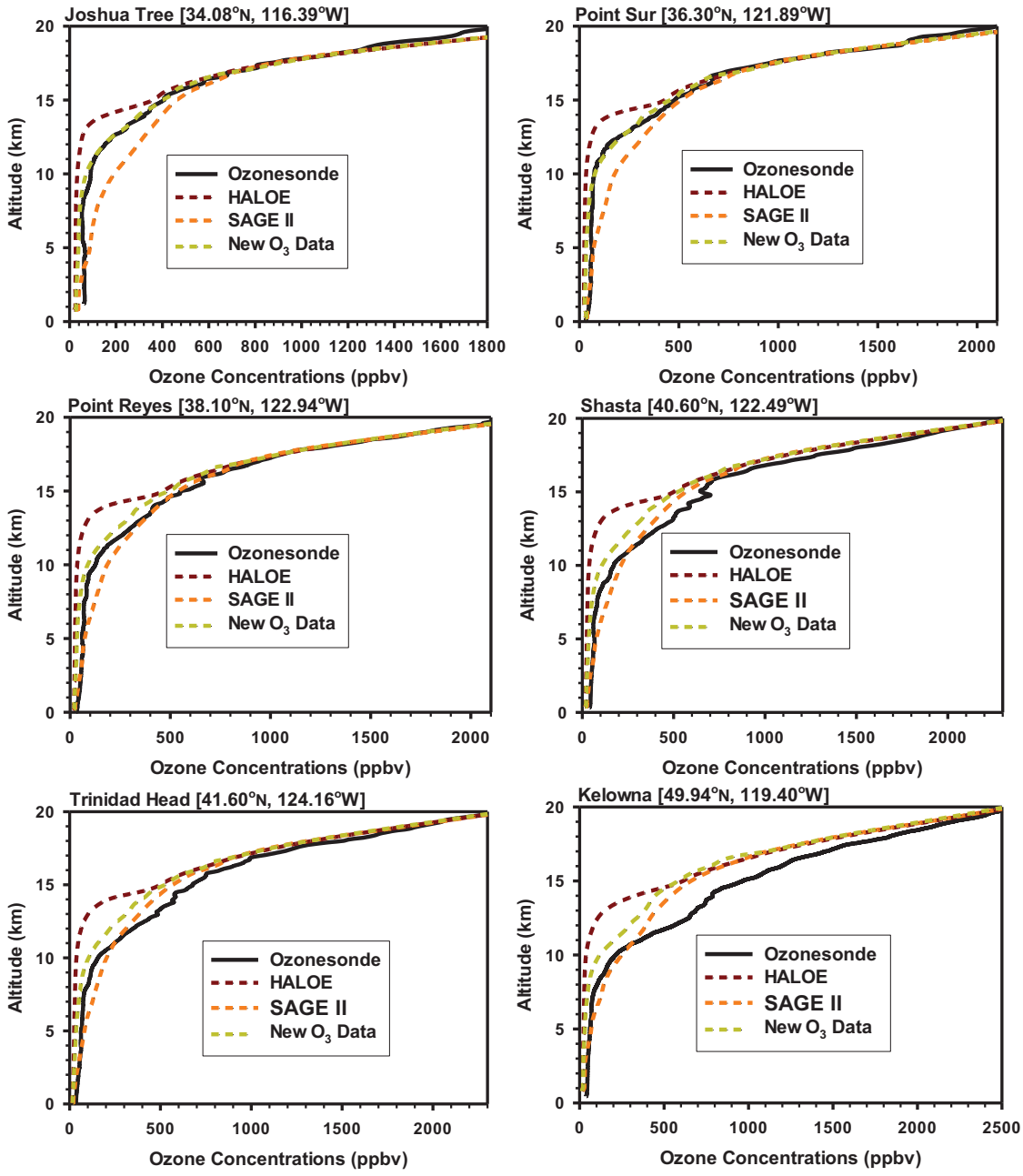

Fig. 16. Ozone model performance compared with measurements at six ozonesonde sites during the 2010 CalNex field study, using data from HALOE, SAGE II and this new ozone climatology, respectively, as upper boundary conditions.